Bond-order-wave phase and quantum phase transitions in the one-dimensional extended Hubbard model

Pinaki Sengupta
Department of Physics, University of Illinois at Urbana-Champaign, 1110 West Green Street, Urbana, Illinois 61801

Anders W. Sandvik
Department of Physics, Åbo Akademi University, Porthansgatan 3, FIN-20500 Turku, Finland

David K. Campbell
Departments of Physics and of Electrical and Computer Engineering, Boston University, 44 Cummington Street, Boston, Massachusetts 02215

(Received 2 December 2001; published 1 April 2002)

We use a stochastic series-expansion quantum Monte Carlo method to study the phase diagram of the one-dimensional extended Hubbard model at half-filling for small to intermediate values of the on-site U and nearest-neighbor V repulsions. We confirm the existence of a novel, long-range-ordered bond-order-wave (BOW) phase recently predicted by Nakamura [J. Phys. Soc. Jpn. **68**, 3123 (1999)] in a small region of the parameter space between the familiar charge-density-wave (CDW) state for $V \gtrsim U/2$ and the state with dominant spin-density-wave (SDW) fluctuations for $V \lesssim U/2$. We discuss the nature of the transitions among these states and evaluate some of the critical exponents. Further, we determine accurately the position of the multicritical point, $(U_m, V_m) = (4.7 \pm 0.1, 2.51 \pm 0.04)$ (in energy units where the hopping integral is normalized to unity), above which the two continuous SDW-BOW-CDW transitions are replaced by one discontinuous (first-order) direct SDW-CDW transition. We also discuss the evolution of the CDW and BOW states upon hole doping. We find that in both cases the ground state is a Luther-Emery liquid, i.e., the spin gap remains but the charge gap existing at half-filling is immediately closed upon doping. The charge and bond-order correlations decay with distance r as r^{-K_ρ}, where K_ρ is approximately 0.5 for the parameters we have considered. We also discuss advantages of using parallel tempering (or exchange Monte Carlo)—an extended ensemble method that we here combine with quantum Monte Carlo—in studies of quantum phase transitions.

DOI: 10.1103/PhysRevB.65.155113 PACS number(s): 71.10.−w, 71.27.+a, 71.30.+h, 05.30.−d

I. INTRODUCTION

The one-dimensional (1D) extended Hubbard model has been extensively studied in recent years, both as an important theoretical test bed for studying novel concepts in 1D (e.g., spin-charge separation), methods, (e.g., quantum Monte Carlo, exact diagonalization, and the density-matrix renormalization group) and as a useful model for several classes of quasi-1D materials including copper-oxide materials related to the high-Tc cuprate superconductors,[1] conducting polymers,[2] and organic charge-transfer salts.[3] General 1D extended Hubbard models differ from the standard Hubbard model, which includes only an on-site electron-electron interaction U, by the addition of longer-range interactions that are necessary to explain several experimentally observed effects in real materials, e.g., excitons in conducting polymers. The simplest extended Hubbard model (henceforth, EHM), on which we focus in this paper, consists of adding a nearest-neighbor interaction V. If the interaction parameters are assumed to arise solely from Coulomb interactions, both U and V are repulsive (positive), and $U > V$. However, viewed as phenomenological parameters incorporating the effects of additional (e.g., electron-phonon) interactions, the ranges of these parameters can be much broader, including $U, V < 0$. The Hamiltonian is

$$H = -t \sum_{i,\sigma} (c^{\dagger}_{i+1,\sigma} c_{i,\sigma} + \text{H.c.}) + U \sum_i \left(n_{i,\uparrow} - \frac{1}{2} \right) \left(n_{i,\downarrow} - \frac{1}{2} \right) + V \sum_i (n_{i+1} - 1)(n_i - 1) - \mu \sum_i n_i , \quad (1)$$

where $c^{\dagger}_{i,\sigma}$ ($c_{i,\sigma}$) creates (annihilates) an electron with spin σ at site i, t is the hopping integral between adjacent sites and μ is the chemical potential. Henceforth we set $t = 1$ and express the interaction parameters U and V in units of t.

The ground-state phase diagram of the EHM at half-filling ($\mu = 0$) has been extensively studied using both analytical and numerical methods. Despite the apparent simplicity of the model, the phase diagram shows surprisingly rich structure. In the limit $V = 0$ (the standard Hubbard model), the Hamiltonian (1) can be diagonalized exactly using the generalized Bethe ansatz.[4] For $V \neq 0$, the model has been studied using perturbative methods and numerical simulations.[5–15] Broadly, the phase diagram consists of insulating phases with dominant charge-density-wave (CDW) and spin-density-wave (SDW) characters and metallic phases where singlet and triplet superconducting correlations dominate. In the physically relevant region for ''Coulomb-only'' parameters ($U, V > 0$), the system is in a CDW phase for large V/U and in a state with dominant SDW fluctuations for small V/U. The CDW phase has broken discrete symmetry, character-

 ©2002 The American Physical Society

ized predominantly by alternating doubly occupied and empty sites and exhibits long-range order. The SDW phase, on the other hand, has continuous symmetry and hence cannot exhibit long-range order in 1D (by the Mermin-Wagner theorem). Instead, it is a critical state characterized by the slow (algebraic) decay of the staggered spin-spin correlation function. Indeed, in the limit $U \gg 1$, $U \gg V$, the model reduces to an effective Heisenberg model with $J \sim 1/(U-V)$. For small U and V ($U,V \ll 1$), the boundary between the CDW and the SDW phases was predicted to be at $U=2V$ using weak-coupling renormalization-group techniques ("g-ology").[6,7] Strong-coupling calculations using second-order perturbation theory also gave the same phase boundary ($U=2V$) between the CDW and the SDW phases for large U and V ($U,V \gg 1$).[5,6] For intermediate values of the parameters, the phase boundary was found to be shifted slightly away from the $U=2V$ line such that the SDW phase is enhanced, as shown by quantum Monte Carlo simulations[8,9] as well as strong coupling calculations using perturbation theory up to the fourth order.[12] Moreover, the nature of the transition is quite different in the two coupling regions, changing from continuous (second-order) in the weak-coupling limit to discontinuous (first-order) in the strong-coupling limit. Estimates for the location of the multicritical point, where the nature of the transition changes, have ranged from $U_m \simeq 1.5$ to $U_m \simeq 5$ (and $V_m \approx U_m/2$).[8–11,14] Despite the broad uncertainty in the actual value of the tricritical point, the phase diagram was believed to be well understood.

Recently, however, by studying the EHM ground-state broken symmetries using level crossings in excitation spectra obtained by exact diagonalization, Nakamura[16] has argued for the existence of a novel bond-order-wave (BOW) phase for small to intermediate values of U and V in a narrow strip between the CDW and the SDW phases. The BOW phase is characterized by alternating strengths of the expectation value of the kinetic-energy operator on the bonds. It is predicted to be a state where the discrete (twofold) symmetry is broken and should hence exhibit true long-range order. Nakamura thus argues that the transition between CDW and SDW phases in this region is replaced by two separate transitions: (i) a continuous transition from CDW to BOW; and (ii) a Kosterlitz-Thouless spin-gap transition from BOW to SDW. The BOW region vanishes at the multicritical point beyond which the transition between CDW and SDW phases is direct and discontinuous. A schematic phase diagram including Nakamura's BOW state is shown in Fig. 1.

Considering the long history of the 1D EHM and the large number of studies of the $U \approx 2V$ region with a variety of analytical and numerical tools, the proposal of a new phase is certainly remarkable. Importantly, the level-crossing method used by Nakamura cannot by itself exclude the conventional scenario of a direct SDW-CDW transition for the whole range of $U,V>0$; a level crossing corresponding to this transition was also found[16] between the SDW-BOW and BOW-CDW crossing curves. The position of the BOW-CDW level crossing is, however, in closer agreement with the strong-coupling result for the vanishing of the CDW order, and this was taken as evidence of a long-range-ordered BOW in the ground state for certain parameters. It is important to confirm this hitherto undiscovered phase using other methods.

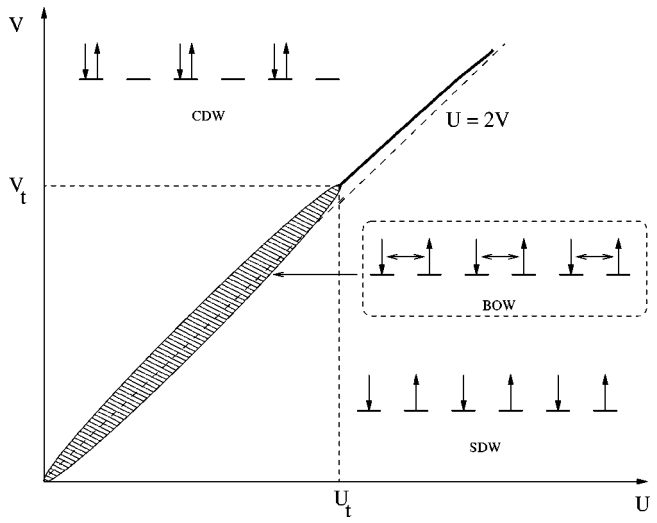

FIG. 1. Schematic ground-state phase diagram of the EHM at half-filling, as proposed by Nakamura. The CDW and BOW phases are long range ordered (broken symmetry), whereas the SDW phase has no broken symmetry but exhibits an algebraically decaying spin-spin correlation function.

To attempt this confirmation, we have used the highly efficient stochastic series-expansion (SSE) quantum Monte Carlo method[17–19] to study the EHM at half-filling in the vicinity of $U=2V$. This method allows us to probe directly the spin-, charge-, and bond-order correlations in the ground state of lattices with more than one hundred sites (up to 256 sites were used in this study). Using finite-size scaling techniques for the various order parameters, we confirm the existence of a BOW state with spin and charge gaps in a region very close to that predicted by Nakamura for small U,V. We also further improved the SSE simulations by applying a quantum version of the thermal-parallel-tempering scheme (or exchange Monte Carlo) (Refs. 20–22) for simulations close to and across the phase boundaries. This "quantum parallel tempering" greatly reduced the effects of "sticking"—where the simulation gets trapped in the wrong phase close to a phase boundary—and was found to be particularly useful for the discontinuous (first-order) direct SDW-CDW transition. As a consequence, we were able to obtain a more accurate estimate for the location of the multicritical point (U_m, V_m) where the BOW phase vanishes and is replaced by a first-order SDW-CDW transition line. As we discuss below, we find $U_m = 4.7 \pm 0.1, V_m = 2.51 \pm 0.04$.

In order to investigate the possibility of soliton lattices forming out of the long-range CDW and BOW states when doping away from half-filling, we have also carried out some simulations of lightly doped systems. We find that in both cases the ground state is a Luther-Emery liquid, with a spin gap and slow algebraic decay ($\sim r^{-K_\rho}$, with $K_\rho \approx 0.5$) of the dominant CDW and BOW correlations.

The remainder of the paper is organized into four sections and two appendixes. In Sec. II we briefly sketch the SSE method and introduce the different observables we study. In Sec. III we present the results of our simulations at half-

filling and discuss their interpretation. Doped systems are considered in Sec. IV. We conclude with a brief summary in Sec. V. In Appendix A we present some important details of the extension of the SSE method to allow efficient loop updates for fermions. We illustrate the advantages of the quantum-parallel-tempering scheme in Appendix B.

II. NUMERICAL METHODS AND OBSERVABLES

A. The SSE method and its fermion loop-update extension

The SSE method[17,18] is a finite-temperature quantum Monte Carlo method based on importance sampling of the diagonal elements of the Taylor expansion of $e^{-\beta H}$, where β is the inverse temperature $\beta = t/T$. Ground-state expectation values can be obtained using sufficiently large values of β, and there are no approximations beyond statistical errors. Recently, in the context of spin systems,[19] an efficient ''operator-loop update'' was developed to sample the operator sequences appearing in the expansion. The resulting method has proven to be very efficient for several different models.[23–25] To apply the most efficient variant of SSE method to the EHM, we need to generalize the previous operator-loop-update scheme to spinful fermions. This is an important extension, but because of its technical nature we have relegated our detailed discussion of it to an appendix.

We have applied the SSE algorithm to the 1D EHM for system sizes ranging from $N=8$ to 256 sites, with maximum inverse temperatures β chosen appropriately to isolate the ground state. We have verified the correctness of the simulation code by comparing $N=8$ results with exact-diagonalization (Lanczos) results.

Although the operator-loop update is indeed significantly more efficient than previous local updates for sampling of the SSE configurations, we still have problems with ''trapping'' close to a first-order phase transition, i.e., the simulation can get stuck in the wrong phase very close to the critical point. There are also problems with slow dynamics in long-range-ordered phases with a broken discrete symmetry (such as, BOW or CDW phases). In order to overcome these problems we have developed a ''quantum-parallel-tempering'' scheme—a generalization of the thermal-parallel-tempering method[20–22] commonly used to equilibrate classical spin glass simulations. The method amounts to running several simulations on a parallel computer, using a fixed value of U and different but closely spaced values of V at and around the critical value V_c. Along with the usual Monte Carlo updates, we attempt to swap the configurations for processes with adjacent values of V at regular intervals (typically after every Monte Carlo step) according to a scheme that maintains detailed balance in the space of the parallel simulations, as explained in Appendix B. In contrast with Ref. 22, we here find parallel tempering to be particularly useful in studying the first-order transition, where the problem of trapping is the most pronounced. In Appendix B we also present a comparative example to illustrate the improvement obtained by parallel tempering.

B. Observables

In addition to the ground-state energy, $E=\langle H\rangle/N$, the observables we study include the static structure factors and susceptibilities corresponding to the different phases (CDW, SDW, and BOW). The structure factors are given by

$$S_{SDW}(q)=\frac{1}{N}\sum_{j,k} e^{iq(j-k)}\langle S_j^z S_k^z\rangle,$$

$$S_{CDW}(q)=\frac{1}{N}\sum_{j,k} e^{iq(j-k)}\langle n_j n_k\rangle-\langle n_j\rangle^2,$$

$$S_{BOW}(q)=\frac{1}{N}\sum_{j,k} e^{iq(j-k)}\langle k_j k_k\rangle-\langle k_j\rangle^2, \tag{2}$$

where

$$k_j=\sum_{\sigma=\uparrow,\downarrow}(c^\dagger_{j+1,\sigma}c_{j,\sigma}+\text{H.c.}) \tag{3}$$

is the kinetic-energy operator associated with the jth bond. The corresponding static susceptibilities are given by

$$\chi_{SDW}(q)=\frac{1}{N}\sum_{j,k} e^{iq(j-k)}\int_0^\beta d\tau\langle S_j^z(\tau)S_k^z(0)\rangle \tag{4}$$

and analogous expressions for $\chi_{CDW}(q)$ and $\chi_{BOW}(q)$. Since all the phases mentioned have a period 2, the staggered structure factor and susceptibilities are the most important observables. We define order parameters for the phases in terms of the staggered structure factors

$$m_\alpha=\sqrt{S_\alpha(\pi)/N}, \tag{5}$$

where $\alpha=$ CDW, SDW, or BOW. We have also studied the charge stiffness constant ρ_c. It is defined as the second derivative of the internal energy per site, E, with respect to a twist ϕ (Ref. 26),

$$\rho_c=\frac{\partial^2 E(\phi)}{\partial\phi^2}, \tag{6}$$

under which the hopping term in the Hamiltonian (1) is replaced by

$$k_c(\phi)=-t\sum_{j,\sigma}(e^{-i\phi}c^\dagger_{j+1,\sigma}c_{j,\sigma}+\text{H.c.}). \tag{7}$$

The spin stiffness constant ρ_s is defined by a similar expression, with the hopping term now being replaced by

$$k_s(\phi)=-t\sum_{j,\sigma}(e^{-i\phi_\sigma}c^\dagger_{j+1,\sigma}c_{j,\sigma}+\text{H.c.}), \tag{8}$$

with $\phi_\uparrow=-\phi_\downarrow=\phi$. In the framework of the SSE method, the estimators for the charge and spin stiffness are given in terms of expectation values of squared winding numbers (see Appendix A).

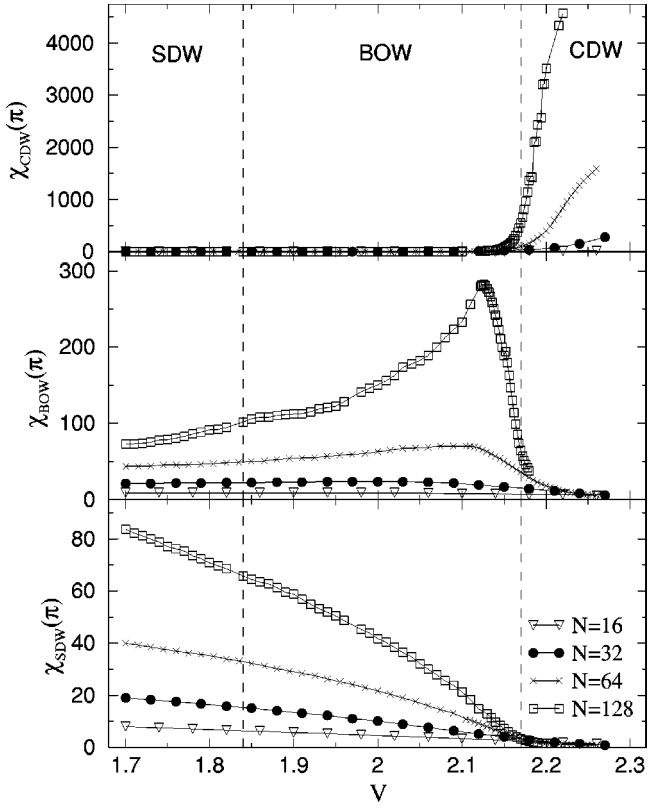

FIG. 2. The variation with V (at fixed $U=4$) of the staggered susceptibilities (CDW, BOW, and SDW, from the top) in the neighborhood of the BOW phase predicted by Nakamura (the vertical dashed lines show the predicted SDW-BOW and BOW-CDW boundaries). The statistical errors are typically of the order of the size of the symbols (slightly larger for the $N=128$ CDW at high V). The scans for $N=16$ and 32 were obtained in single parallel-tempering simulations, whereas those for $N=64$ and 128 consisted of two and four nonoverlapping runs, respectively.

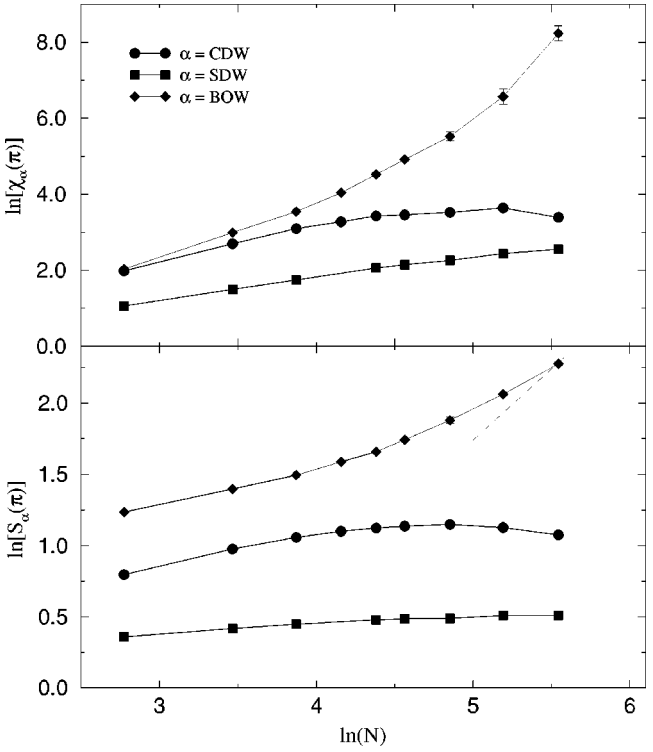

FIG. 3. $\ln[\chi(\pi)]$ and $\ln[S(\pi)]$ vs $\ln[N]$ for the different phases at $U=4$, $V=2.14$, and system sizes N up to 256. The dashed line in the $S(\pi)$ panel has slope 1.

III. RESULTS AT HALF-FILLING

As noted above, we have studied chains with N up to 256 with periodic boundary conditions.[27] Typically, an inverse temperature of $\beta=2N$ was sufficient for the calculated properties to have converged to their ground-state values, except in the case of $N=256$, for which $\beta=4N$ was needed for some quantities. In this section we first discuss our evidence for the existence of a long-range BOW phase, then our analysis of the continuous BOW-CDW and SDW-BOW transitions for small (U,V), the discontinuous SDW-CDW transition for large (U,V), and finally our determination of the location of the multicritical point separating these transitions.

A. Existence of the BOW phase

Plots of the variation of the staggered susceptibilities corresponding to the three different phases—CDW, SDW, and BOW—show the existence of strong BOW fluctuations in a region with $V\simeq U/2$ in parameter space where Nakamura predicted a BOW state. Figure 2 is one such plot for $U=4$ and $1.7\leqslant V<2.3$. In a long-range-ordered phase (BOW, CDW), the corresponding $\chi(\pi)$ is expected to diverge with increasing system, whereas the other two susceptibilities should converge to constants. In the SDW phase there is no long-range order but algebraically decaying correlations of both SDW and BOW nature; hence $\chi_{SDW}(\pi)$ and $\chi_{BOW}(\pi)$ should both diverge here, but the BOW divergence should be much slower than in the long-ranged BOW phase. These behaviors are indeed seen in Fig. 2, with the susceptibilities for SDW, BOW, and CDW dominating in turn as V is increased. The BOW-CDW phase boundary can be quite well resolved, since it involves a standard second-order (continuous) phase transition. On the other hand, the SDW-BOW boundary is more difficult to locate, for it involves a Kosterlitz-Thouless transition in which the spin gap opens exponentially slowly as one enters the BOW phase,[16] resulting in only a slow decay of the staggered SDW susceptibility in the BOW phase for the system sizes accessible in our work.

Figure 3 shows $\ln[\chi_\alpha(\pi)]$ and $\ln[S_\alpha(\pi)]$ vs $\ln[N]$ for the parameters $(U,V)=(4,2.14)$ for which the ground state should be inside the BOW phase. We find that both $\chi_{BOW}(\pi)$ and $S_{BOW}(\pi)$ diverge strongly with the system size, whereas the structure factor and susceptibility corresponding to CDW have a maximum and then decrease with the system size for large N. The SDW structure factor appears to have converged for $N=256$ but the susceptibility still shows a weak growth—in a spin-gapped BOW phase it should eventually converge, too, but if the gap is very small the convergence occurs only for much larger systems. The growth with N seen here is much slower than N, which should be the asymptotic behavior in an SDW phase for any spin rotationally invariant

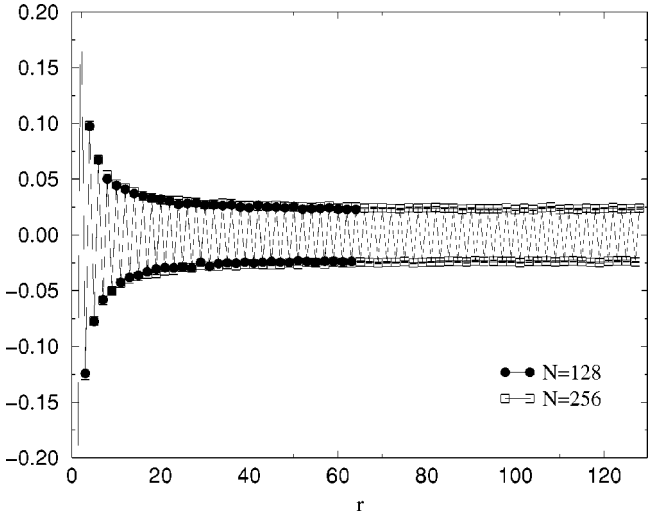

FIG. 4. Real-space BOW correlation function at $U=4$, $V=2.14$ for system sizes $N=128$ and 256.

1D system,[28] and the growth slows with increasing N. Hence an asymptotic divergence of $\chi_{SDW}(\pi)$ can be excluded. The dominant asymptotic characteristic of the ground state is clearly BOW. The system sizes considered are not large enough for $S_{BOW}(\pi)$ to have reached the asymptotic behavior $\sim N$ expected if there is long-range order, which we will explain further below. The very fast divergence of $\chi_{BOW}(\pi)$ is expected on account of the twofold degenerate BOW ground state. For finite N this degeneracy is not perfect, but an exponentially fast closing of the gap between the symmetric and antisymmetric linear combinations of the two asymptotically degenerate symmetry-broken ordered states can be expected, which would eventually cause $\chi_{BOW}(\pi)$ to diverge exponentially.

The most direct evidence for a long-range BOW comes from the the real-space kinetic-energy correlation function

$$C_{BOW}(r)=\frac{1}{N}\sum_{i=1}^{N}\langle k_i k_{i+r}\rangle-\langle k_i\rangle^2. \tag{9}$$

As seen in Fig. 4, this correlation function oscillates with period 2 and its magnitude decays considerably for short distances. For long distances there is a convergence to a constant, nonzero magnitude, which is the same within statistical errors for $N=128$ and 256. The significant enhancement of the correlations at short distances explains the deviations from the expected asymptotic linear scaling of the integrated correlation function, $S_{BOW}(\pi)$, for the system sizes shown in Fig. 3.

Further proof of the existence of the BOW phase is obtained by looking for spin and charge gaps in this region. Instead of calculating the gaps directly, which cannot easily be done to high accuracy for large system sizes, we use the following indirect method: It is known[28] that if the ground state of a 1D system is gapless in the spin sector, the Luttinger liquid parameter K_σ governing the asymptotic equal-time spin-correlation function is $K_\sigma=1$.[14] It has been further shown[29] that the slope $S_{SDW}(q)/q$ gives K_σ/π in the limit $q\to 0$. Hence, $S_{SDW}(q)/q\to 1/\pi$ as $q\to 0$. On the other hand,

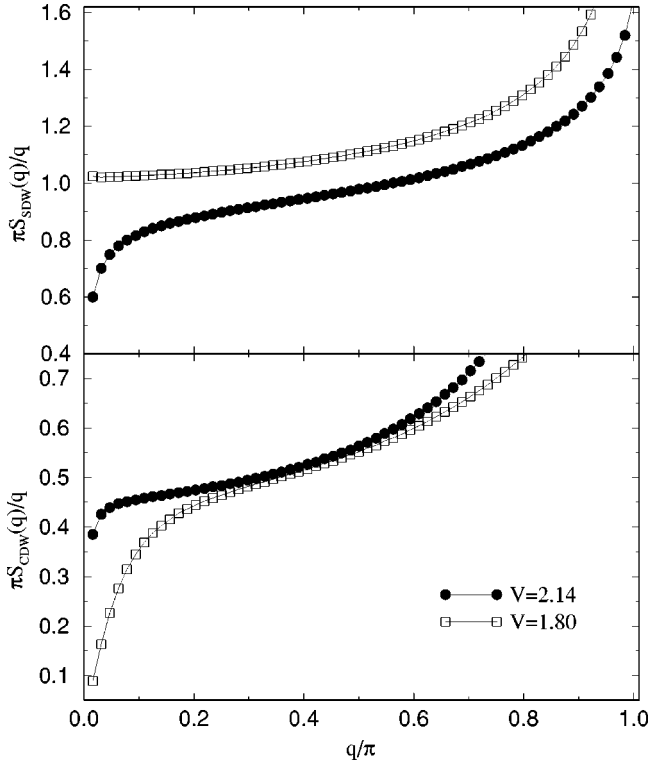

FIG. 5. $S_{SDW}(q)/q$ and $S_{CDW}(q)/q$ vs q for $U=4$ and $V=2.14$ and $V=1.8$ ($N=128$).

if the ground state has a spin gap, $S_{SDW}(q)/q\to 0$ as $q\to 0$. With this criterion, even a very small spin gap can be detected, since it is, in practice, sufficient to see that $\pi S_{SDW}(q)/q$ decays below 1 for small q to conclude that $K_\sigma\neq 1$ and hence that a spin gap must be present. Similarly, for a ground state with no charge gap, $\pi S_{CDW}(q)/q\to K_\rho$ as $q\to 0$, whereas if the ground state does have a charge gap, $S_{CDW}(q)/q\to 0$ as $q\to 0$. Unlike K_σ, where the value is fixed at 1 for spin rotationally invariant systems, the Luttinger liquid charge correlation parameter K_ρ is a function of U and V, and its precise value for given U and V is not known [except at $V=0$ (Ref. 30)]. Due to the logarithmic corrections typical for 1D systems, it is very difficult to observe numerically that $\pi S_{SDW}(q)/q$ becomes exactly 1.[31–33] Empirically, we have found that in the gapless case the value 1 is always approached from above (which is the case also for spin systems[32]), and hence the detection of the spin gap using this quantity is not hampered by the log corrections—if $\pi S_{SDW}(q)/q$ decays below 1 one can conclude that here is a gap.

Figure 5 shows $\pi S_{SDW}(q)/q$ and $\pi S_{CDW}(q)/q$ vs q/π for $U=4$ and two values of V. One of the points ($V=2.14$) is inside the BOW phase, whereas the other ($V=1.8$) is in the SDW phase. The $\pi S_{SDW}(q)/q$ curve for $V=1.8$ is close to 1 for a wide range of q values, whereas the $V=2.14$ curve exhibits a sharp drop as $q\to 0$ indicating, respectively, the absence and the presence of a spin gap. Similarly, the evidence for a vanishing limit of $S_{CDW}(q)/q$ and hence of a charge gap for $V=1.8$ is clear. Since the point $V=2.14$ is quite close to the critical point ($V_c=2.16$), where

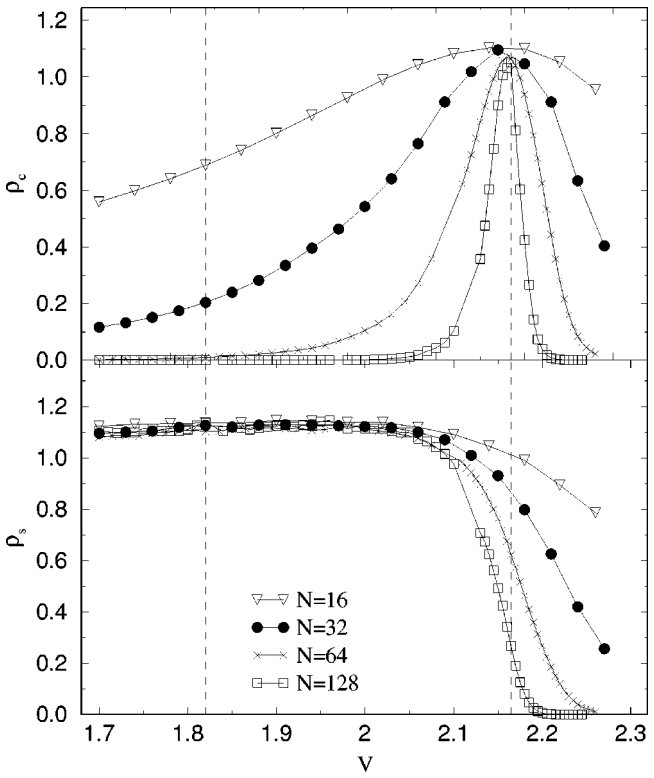

FIG. 6. Behavior of the charge and spin stiffness across the BOW-CDW boundary for $U=4$. The upper(lower) panel shows the charge(spin) stiffness. The vertical dashed lines indicate the position of the phase boundaries according to Nakamura.

the charge gap vanishes, the magnitude of the gap is very small and we need to go to still smaller q, i.e., larger system size, to see a pronounced effect like that for $V=1.8$. Nevertheless, the downturn for the smallest q is a good indication of a gap.

The opening of spin and charge gaps can also be detected in the spin and charge stiffness constants, which should vanish as $N\rightarrow\infty$ if there are gaps. The asymptotic charge stiffness should hence be nonzero only exactly at the BOW-CDW phase boundary. The spin stiffness should be (1) nonzero in the SDW phase, (2) approach a constant value exactly at the phase boundary (with logarithmic size corrections),[34,35] and (3) vanish inside the CDW phase. In Fig. 6 we show the stiffness constants for $U=4$ in the neighborhood of the BOW phase. As expected, the charge stiffness peaks at the BOW-CDW phase boundary and decreases rapidly away from it, confirming the vanishing of the charge gap only at the phase boundary. The peak becomes very sharp for large system sizes, and the finite-size corrections to its location are small. We find this the most accurate way to locate the BOW-CDW phase boundary. The spin stiffness is clearly zero in the CDW phase, and a sharp decrease with increasing N is also seen for V values well inside the BOW phase. Since the spin gap opens up exponentially slowly at the SDW-BOW boundary it is difficult to locate the transition this way. Our data nevertheless indicate that the BOW phase at $U=4$ may not extend down to the value $V\approx 1.82$ obtained by Nakamura. We will discuss this phase transition and determine the transition point more accurately below, in Sec. III C.

B. BOW-CDW transition

In addition to proving the existence of the BOW phase, we have studied in detail the nature of the continuous BOW-CDW transition for two different values of U ($U<U_m$). For $(U,V)=(U_c,V_c)$, i.e., on the BOW-CDW phase boundary, the real space staggered charge and kinetic-energy correlation functions fall off algebraically as

$$\langle n_i n_{i+r}\rangle(-1)^r\sim r^{-\eta},$$

$$(\langle K_i K_{i+r}\rangle-\langle K_i\rangle^2)(-1)^r\sim r^{-\eta}. \tag{10}$$

Based on conformal-field-theory calculations for similar phase transitions in 1D spin systems,[36] the exponent η can be expected to depend on (U_c,V_c) but should be the same for both the CDW and BOW correlations. This gives the finite-size scaling of the structure factor and the susceptibility at the critical point

$$S_{CDW,BOW}(\pi)\sim N^{1-\eta},$$

$$\chi_{CDW,BOW}(\pi)\sim N^{2-\eta}. \tag{11}$$

With a spin gap but no charge gap, as was demonstrated above, we expect the critical state to be of the Luther-Emery liquid type.[37] The exponent η is then related to the Luttinger liquid parameter K_ρ by $\eta=1-K_\rho$.

Figure 7 presents plots of $\ln[\chi_{CDW}]$ and $\ln[\chi_{BOW}]$ vs $\ln[N]$ for $U=4$ and three different values of V around the critical point, which as discussed above should be close to 2.16. The data points for $V=2.16$ indeed fall almost on straight lines, indicating critical scaling for both the CDW and BOW fluctuations. The value of the critical exponent η, obtained from the slope of the $V=2.16$ curves for both χ_{CDW} and χ_{BOW}, is $\eta\approx 0.5$. The scaling of the structure factors, S_{CDW} and S_{BOW} at $V=2.16$ is also consistent with $\eta\approx 0.5$. It is, however, difficult to extract a precise value for η from this finite-size scaling, due to subleading corrections to the scaling, as well as effects from the fact that the U,V point studied is not exactly on the phase boundary. As was discussed in Sec. III A, the Luttinger liquid parameter K_ρ can also be extracted from the $q\rightarrow 0$ limit of $S_{CDW}(q)/q$. This is, in general, a more accurate method, since the convergence with the system size is faster for the subleading $1/r^2$ contribution to the correlation function, which this estimator accesses.[29,30] Figure 8 shows results for $U=4$ and $U=3$ and the respective critical V values. The $q\rightarrow 0$ behavior gives $K_\rho=0.44\pm 0.01$ for $U=4$, i.e., $\eta=0.56\pm 0.01$, which hence is consistent with the finite-size scaling of the $q=\pi$ quantities. For $U=3$, we obtain $V_c=1.65$, in agreement with Nakamura's result,[16] and the critical exponent $\eta=0.47\pm 0.01$.

C. SDW-BOW transition

The SDW-BOW transition is marked by the opening of a spin gap in the electronic energy spectrum. As argued by

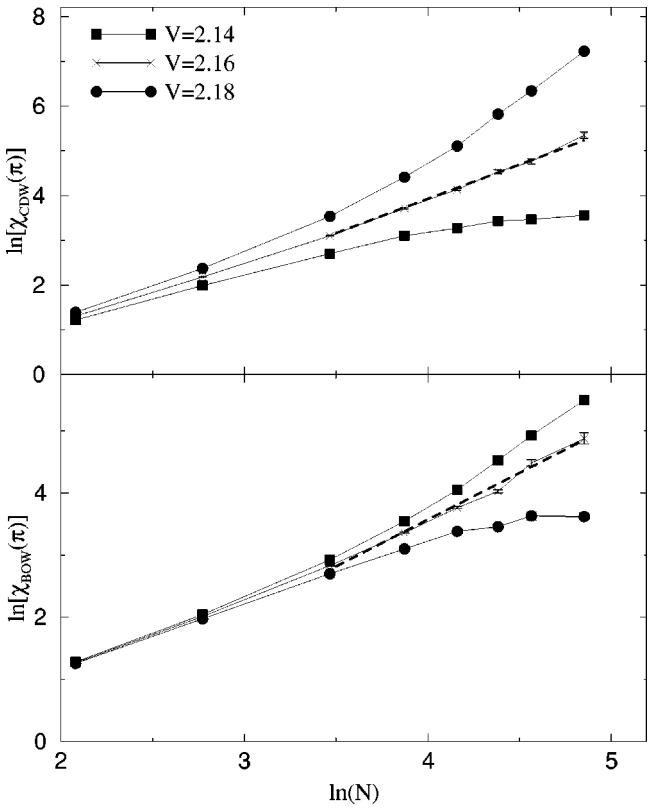

FIG. 7. $\ln[\chi_{CDW}(\pi)]$ and $\ln[\chi_{BOW}(\pi)]$ vs $\ln(N)$ for $U=4$ and different values of V near the critical point. The dashed lines are fits to the $V=2.16$ data.

Nakamura, it is a quantum phase transition of the Kosterlitz-Thouless type and therefore the gap opens up exponentially slowly. This makes it difficult to determine the phase boundary numerically. The numerical data is affected by large finite-size effects that persist up to very large system sizes. As discussed in Sec. III A, the most reliable evidence of the existence of a spin gap is obtained from the behavior of $S_{SDW}(q)/q$ as $q\rightarrow 0$. In practice, an asymptotic value of

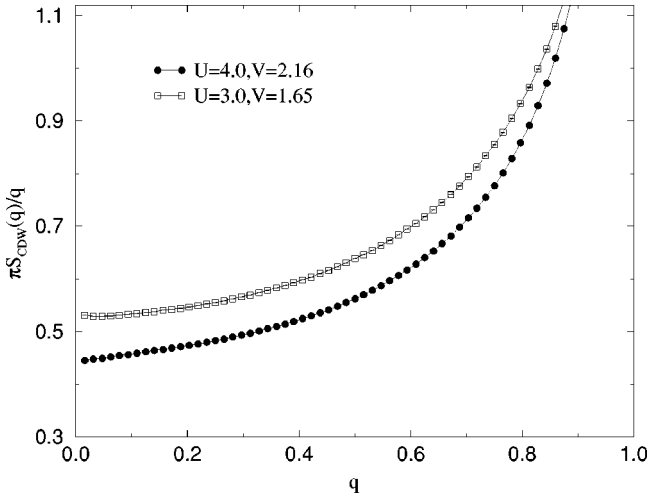

FIG. 8. $\pi S_{CDW}(q)/q$ vs q/π for two points on the BOW-CDW boundary.

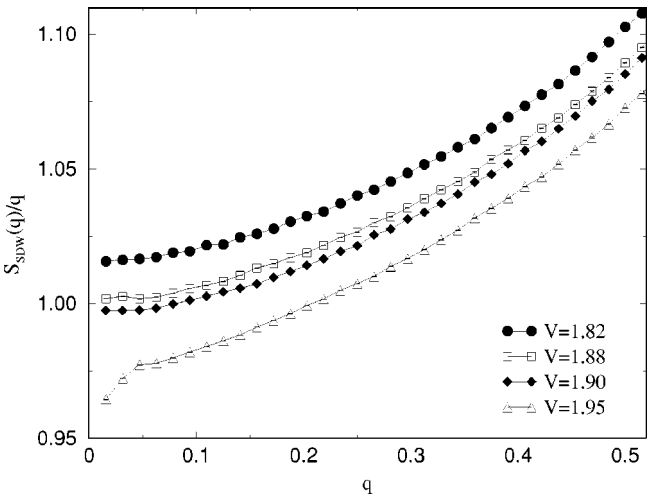

FIG. 9. $S_{SDW}(q)/q$ vs q for $U=4$ and 4 different values of V around the SDW-BOW boundary.

$\pi S_{SDW}(q)/q<1$ as $q\rightarrow 0$ in any (large) system is an indication of the presence of a spin gap in the thermodynamic limit. This allows us to detect the presence of very small spin gaps. Figure 9 shows the behavior of $\pi S_{SDW}(q)/q$ for $U=4$ and different values of V. In the gapless region, logarithmic corrections[32] make it difficult to observe the approach to 1 as $q\rightarrow 0$. In analogy with spin systems,[33] we expect the leading log corrections to vanish at the point where the spin gap opens, and therefore exactly at the critical point there should be a clear scaling to 1. An apparent reduction of the log correction is indeed seen in Fig. 9 as V is increased towards ≈ 1.88. Based on the results, we estimate the SDW-BOW boundary to be at $V=1.89\pm 0.01$ at $U=4$. This is slightly higher than Nakamura's critical value $V=1.82$ for this U. We believe the difference is due to nonasymptotic finite-size effects in the exact diagonalization calculation, which used system sizes only up to $N=14$. Hence, we find that the BOW phase exists in a slightly smaller, while still significant, region of the phase space.

D. First-order SDW-CDW transition

For $U>U_m$, the transition is a discontinuous (first-order) direct SDW-CDW transition with no intervening BOW phase. Figure 10 shows the V dependence of the CDW order parameter, the total energy, and the kinetic energy across the phase boundary for $U=8$, which according to previous studies[8–11,14] should be well within the regime of first-order transitions. The characteristics of a first-order transition are indeed quite apparent. The order parameter and the kinetic energy change rapidly at the transition point $V_c\approx 4.14$. The finite-size effects diminish with increasing N as the results approach the limiting behavior of a discontinuity in the order parameter and the kinetic energy in the thermodynamic limit. The total energy remains continuous, but there is a clear break in slope at the transition.

The size dependence of the BOW order parameter is shown in Fig. 11. It becomes considerably smaller inside the CDW phase than before the transition. This is expected,

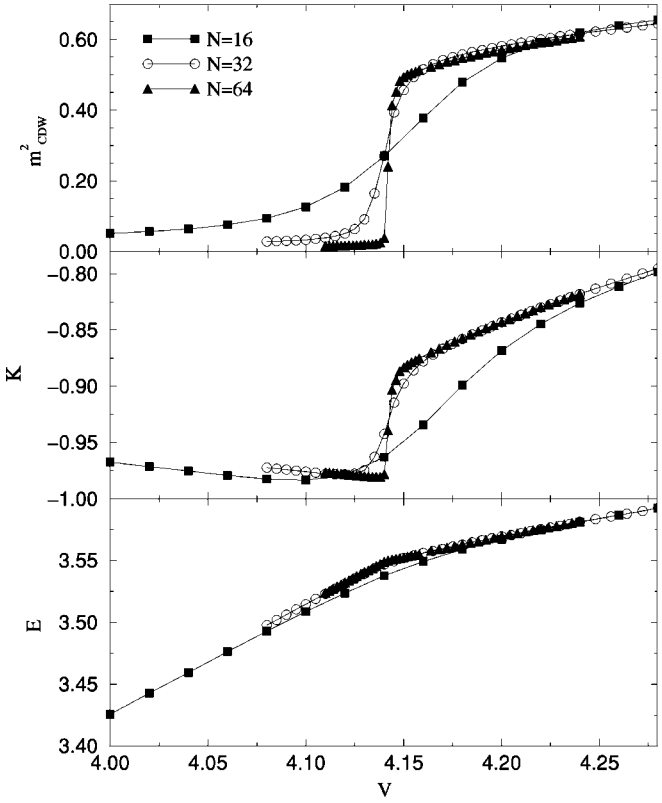

FIG. 10. Behavior of the CDW order parameter, the kinetic energy, and the ground-state energy across the SDW-CDW transition for various system sizes and $U=8$.

since in the SDW phase, but not in the CDW phase, there should be power-law decaying BOW correlations. However, the BOW order parameter decays rapidly with the system size, confirming that there is no long-range BOW for this $U>U_m$.

The behavior with increasingly sharp discontinuities seen in Figs. 10 and 11 indicates a first-order transition due to an avoided level crossing. Note that with increasing chain length the CDW order parameter approaches its thermodynamic value from above for $V<V_c$ and from below for V just above V_c. The curves for different system sizes cross one another in the neighborhood of $V=V_c$ and then once again for a higher V. The second crossing point moves down towards the first one as N increases, whereas the first crossing does not change much with V and appears to be a good criterion for locating the transition point.

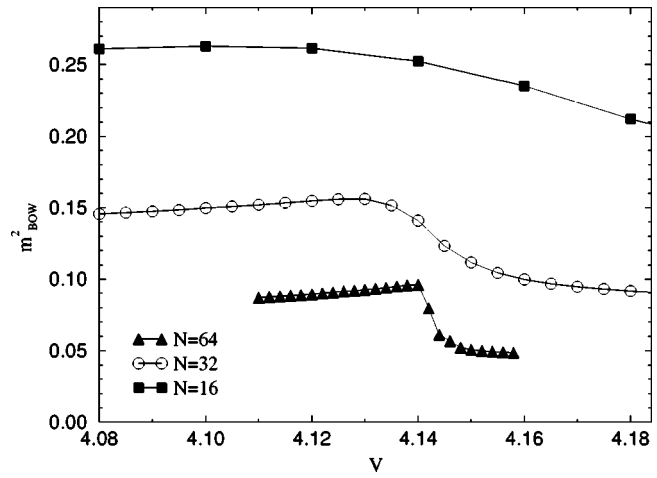

FIG. 11. Behavior of the BOW order parameter across the SDW-CDW transition for various system sizes and $U=8$.

The two curve crossings can be understood as follows: In a transition caused by an avoided level crossing, a crossing of the order-parameter curves close to the critical coupling (approaching the critical coupling as $N\to\infty$) can be expected since the low-energy levels corresponding to an ordered and disordered state swap characters within a parameter range $V\pm\Delta_V(N)$, with $\Delta_V(N)\to 0$ as $N\to\infty$. This behavior is seen clearly in Fig. 10. The finite-N ground state starts to develop CDW characteristics at $V-\Delta_V(N)$ and thus, for a fixed $V<V_c$, the CDW order parameter decreases with increasing N. An analogous argument for fixed $V>V_c$ close to V_c suggests that, in this case, the CDW order must increase with increasing N. On the other hand, for $V\gg V_c$ the real-space CDW correlations are enhanced at short distances (in the same way as the BOW correlations shown in Fig. 4) and for small system sizes there is also some enhancement of the long-distance correlations due to the periodic boundary conditions.[38] Hence, one can expect the CDW order parameter, when defined and measured in terms of its squared expectation Eq. (5), to again *decrease* with N for $V\gg V_c$ and this explains the second crossing of the order-parameter curves seen in Fig. 10.

E. Multicritical point

Although the existence of the tricritical point (which, in view of the existence of the BOW phase, we refer to as the multicritical point) separating the first-order and continuous transition to the CDW state has long been known, its location in the (U,V) plane has not previously been determined accurately using large system sizes. Hirsch[8,9] estimated a value of $U_m=3$ using world line Monte Carlo. Cannon and Fradkin[10] obtained $U_m=1.5$ using field-theory techniques and world lines. Later Cannon, Scalettar, and Fradkin[11] obtained a value of $U_m=3.5$–5 using finite-size scaling of Lanczos results. Using a combination of bosonization and renormalization-group (RG) techniques, Voit[14] obtained $U_m=4.76$. However, as Voit also pointed out, the validity of bosonization and RG, which are applicable in the limit $U,V\to 0$, for intermediate values of the parameters is *a priori* questionable.

By using larger system sizes and an alternative criterion to distinguish between a continuous transition and a first-order level crossing transition, we have obtained an estimate of the multicritical point that we consider more accurate and reliable than the previous estimates. In contrast to most previous numerical studies, our method is not based on plotting histograms of the order parameter, although we will also present such histograms in the following section. In this section we first exploit the qualitatively different finite-size dependence of the growth of the order parameter close to the transition above and below the multicritical point.

For fixed U, the order-parameter curves for different system sizes cross each other at or very close to the critical point ($V=V_c$) in the case of a first-order transition, as discussed above in Sec. III D. Such a crossing cannot occur at a continuous transition, where instead there should be finite-size scaling governed by Eq. (11). This qualitative difference in the finite-size dependence of the order parameter close to the transition point above and below the multicritical point (U_m, V_m) leads us to expect that in the neighborhood of this point, curves of the order parameter for different chain lengths will closely coincide with one another close to $V=V_c$, and U_m is the point at which the curves barely touch each other. When the system size becomes sufficiently large one can also directly observe discontinuities developing when $U>U_m$, in the order parameter as well as in other quantities, as in Fig. 10. In practice this criterion, or any other criterion known to us, cannot be expected to be useful very close to the multicritical point, where the transition is only weakly first order and very large lattices are needed to detect discontinuities developing from avoided level crossings.

Figure 12 shows the finite-size dependence of the CDW order parameter across the transition for three different values of U. For $U=4.2$, only the $N=16$ curve crosses the other curves, and this occurs far from the critical point (as determined using the peak in the charge stiffness, as discussed in Sec. III A). The noncrossing for larger system sizes show that the transition must be continuous at this U. For $U=5.2$, all curves show a crossing behavior and a discontinuity can also be seen developing for the largest system size, i.e., the transition is here of first order. The curves for $U=4.6$ closely follow the expected behavior at the multicritical point, with the curves for the largest systems barely touching each other. Based on data, also for other values of U, we estimate the multicritical point to be $(U_m=4.7\pm0.1, V_m=2.51\pm0.04)$. This agrees very well with Voit's estimate $(U_m=4.76)$.[14] However, it is not clear whether this agreement is fortuitous or whether there is some underlying symmetry that renders bosonization and RG (that assumes $U,V\ll 1$) applicable close to the multicritical point.

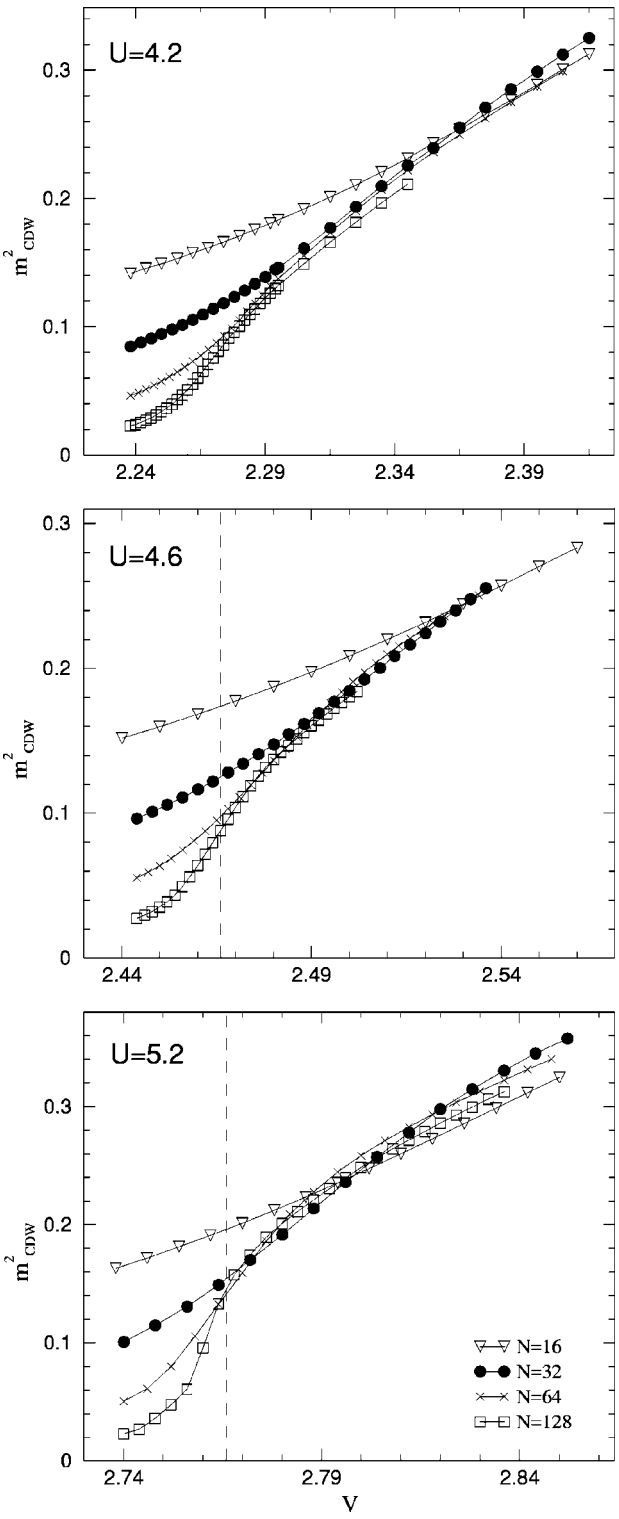

FIG. 12. CDW order parameter vs V across the BOW-CDW boundary for several system sizes near the multicritical point. The dashed line shows the position of V_c for the respective U. Statistical errors are smaller than the symbols.

F. CDW order parameter histograms

Previous studies of the multicritical point have exploited the existence of a three-peak structure in the distribution of the CDW order parameter for a discontinuous SDW-CDW transition in the vicinity of the critical point and its absence at a continuous transition.[8] Outside the CDW phase, the distribution of the CDW order parameter is peaked around zero. For a continuous transition to a CDW state this peak splits into two (corresponding to the positive and negative values of the order parameter), which gradually move apart from each other inside the CDW phase. In a first-order transition, on the other hand, the order parameter takes a nonzero value immediately as the CDW phase is entered and hence the two peaks emerge already separated from each other. Furthermore, at the phase boundary the CDW phase coexists with the competing phase, and this is reflected as a central peak remaining in the CDW order-parameter distribution. The position of the multicritical point can then, in principle, be obtained by locating the point where the three-peak structure first appears. In practice, the accuracy of this method is limited by the fact that the discontinuity is very small for a

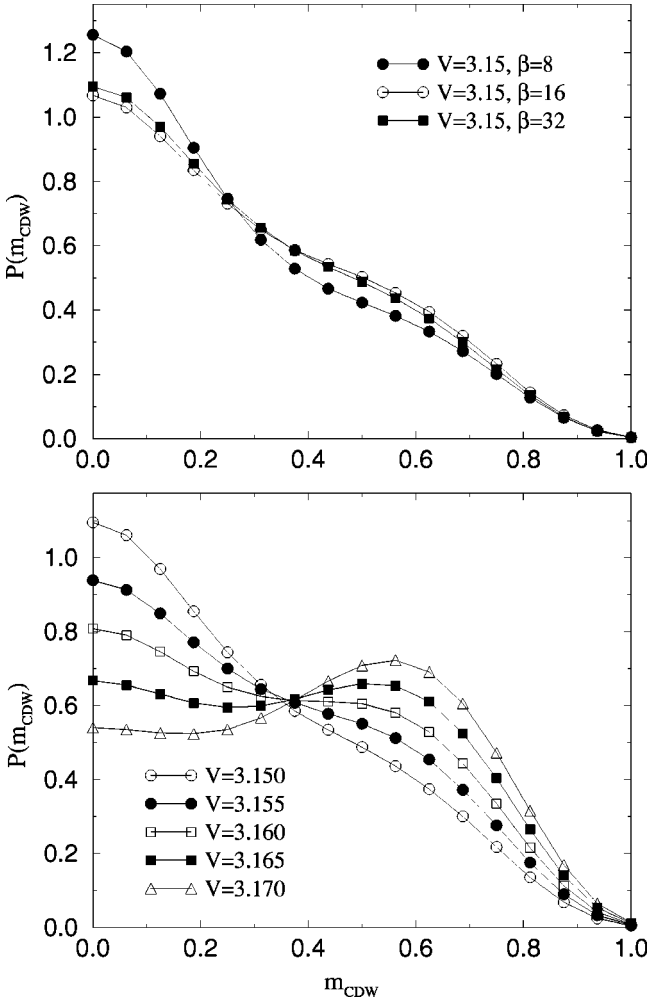

FIG. 13. CDW order-parameter distributions for 32-site systems at $U=6$. Upper panel: Dependence on the inverse temperature β at $V=3.15$. Lower panel: Dependence on V around the first-order phase transition. Statistical errors are of the order of the size of the symbols.

first-order transition close to the multicritical point and very large system sizes are then needed to observe the three peaks. This problem is, of course, common to all methods for distinguishing between a continuous and weakly first-order transition.

In his early QMC study, Hirsch observed a three-peak structure even for U as small as 3 and, therefore, concluded that the transition there is already of first order.[8] For larger U, an unexplained four-peak structure was seen. We have repeated histogram calculations for the lattice size $N=32$ studied by Hirsch. In Fig. 13 we show results for $U=6$, $V=3.15$, where a four-peak structure was seen in the earlier calculation.[8] We only find a central peak, which shows that the system is not in the CDW state for these parameters. There are, however, already signs of side peaks developing, which shows that the system is close to the CDW phase. The significant differences with the earlier result could partially be errors due to the Trotter decomposition used in the world-line simulation method. Temperature effects are only minor, as also shown in Fig. 13. At $\beta=8$, which was used in Ref. 8,

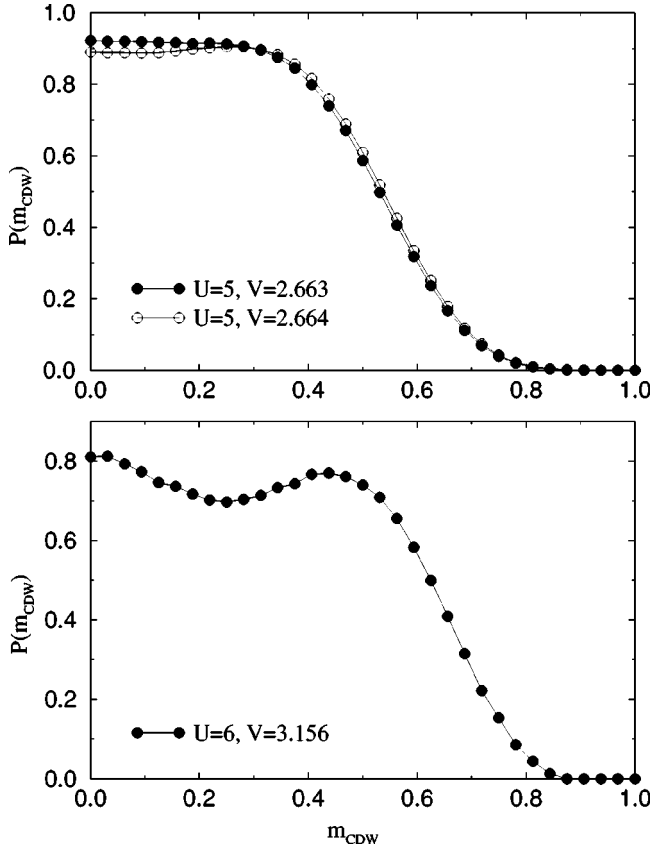

FIG. 14. CDW order-parameter histograms for $N=64$ systems close to the phase transition.

the histogram is only slightly more sharply peaked than at $\beta=16$ and 32. Most likely, the simulation giving the four-peak structure was not sufficiently long, as it consisted of only 10^4 Monte Carlo steps.[8] Even with the more efficient SSE algorithm used in the present work, we find that the autocorrelation times are quite long close to the first-order transition (see Appendix B) and short simulation can produce incorrect order-parameter histograms similar to those shown in Ref. 8. For the histograms shown here, of the order of 10^7–10^8 SSE Monte Carlo steps were used.

In Fig. 13 we also show results for several values of V across the phase transition. A clear three-peak structure (i.e., three peaks in the range $m_{CDW}\in[-1,1]$, of which we only show the positive part) with peaks of almost the same heights can be seen for $V=3.165$. In Fig. 14 we show results for $N=64$. At $U=6$, the three-peak structure appears for $V\approx 3.156$, i.e., at a value slightly lower than for the $N=32$ system. The size of the V region in which three peaks can be observed is also significantly smaller, reflecting the sharpening of the first-order transition caused by an avoided level crossing. At $U=5$, which we have argued above should be close to but above the multicritical point, we do not observe three peaks. However, the histogram becomes very flat for an extended range of m_{CDW}, and the side peak emerges at a finite value of m_{CDW}. This is consistent with the transition still being of first order at $V=5$. Going to still lower V values, the peak just becomes narrower, and it is not possible to definitely conclude this way when the transition becomes continuous.

IV. DOPED SYSTEMS

An interesting question naturally arises from the existence of the Nakamura BOW phase: Can the EHM model support a soliton lattice when doped slightly away from half-filling? Such a state exists in the Su-Schrieffer-Heeger model in the adiabatic limit (with classical, ''frozen'' phonons),[39–41] and also when electron-electron interactions are taken into account.[40,41] In these models, the quantum nature of the phonon field is not taken into account, however. It is known that the dimerized state at half-filling survives even in the presence of quantum fluctuations, at least up to a critical value of the phonon frequency.[42] However, to our knowledge, there have been no reliable numerical calculations addressing the stability of the soliton lattice in the presence of fully quantum-mechanical phonons. The Nakamura BOW is similar to a dimerized lattice with quantum fluctuations, and hence a study of its evolution with hole doping can give insights also into the quantum phonon problem. There are also unresolved issues regarding the doped CDW state.[15] In order to investigate the evolution of the long-range-ordered states upon doping, we have studied the EHM model also away from half-filling, focusing on two parameter values in which the half-filled system is in the BOW (using $U=4$, $V=2.14$) or CDW phase (using $U=4$, $V=2.5$).

We first discuss the effects of doping on the spin and charge gaps in the half-filled CDW and BOW ground states. As in preceding sections, we make use of the behavior of the static structure factor in the limit $q\rightarrow 0$. Figures 15 and 16 show $\pi S_{CDW}(q)/q$ and $\pi S_{SDW}(q)/q$ as a function of q for a range of doping levels, both for parameters where the half-filled system is in the BOW phase (Fig. 15) and in the CDW phase (Fig. 16). From the data we conclude that upon doping away from half-filling, the charge gap vanishes immediately whereas the spin gap survives. This is true for both the CDW and BOW parent states. This behavior is characteristic of a Luther-Emery liquid,[37] in which the charge sector can be described in terms of a Luttinger liquid and the spin sector is gapped. The limiting value of $\pi S_c(q)/q$ as $q\rightarrow 0$ indicates that the Luttinger liquid exponent $K_\rho \approx 0.5$ in both the cases, with only a weak dependence on the doping level for the parameters considered here. Note the crossover behavior occurring in the charge structure at $q\approx 2\pi\delta = 4k_F$ in Fig. 16 (which is accompanied by a peak in the corresponding susceptibility, as will be shown below),[43] reflecting a weak repulsion between dopant holes. No crossover in the charge structure is seen in Fig. 15, where the parent state is a BOW.

Figure 17 shows the variation of the ground-state static susceptibilities for several doping levels in a chain of length $N=128$ for the parameters $U=4, V=2.5$. For $\delta>0$ the charge susceptibility converges to a nonzero value as $q\rightarrow 0$, again showing the absence of a charge gap. Very strong $2k_F$ peaks are evident, and weaker $4k_F$ peaks are also clearly visible. The $2k_F$ peaks diverge with the system size whereas the $4k_F$ peaks are nondivergent, in accord with the Luther-Emery picture. For a Luther-Emery liquid, the charge correlations decay with distance r as r^{-K_ρ},[14] which gives $\chi_{CDW}(2k_F)\sim N^{2-K_\rho}$ for the finite-size scaling of the corresponding $2k_F$ susceptibility. Figure 18 shows the size depen-

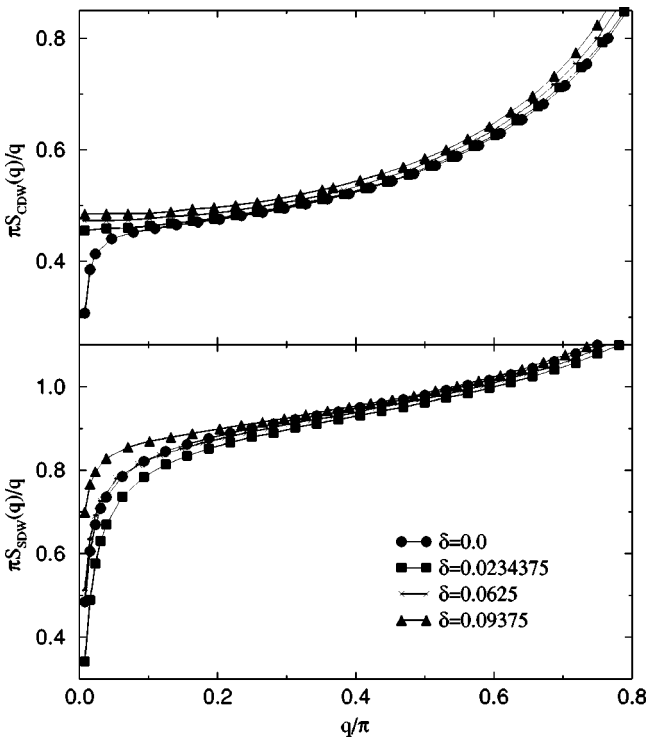

FIG. 15. The static charge (upper panel) and spin (lower panel) structure factor divided by the wave number q as a function of q for 256-site chains at different doping fractions δ. For these parameter values ($U=4, V=2.14$), the half-filled system ($\delta=0$) is in the BOW state.

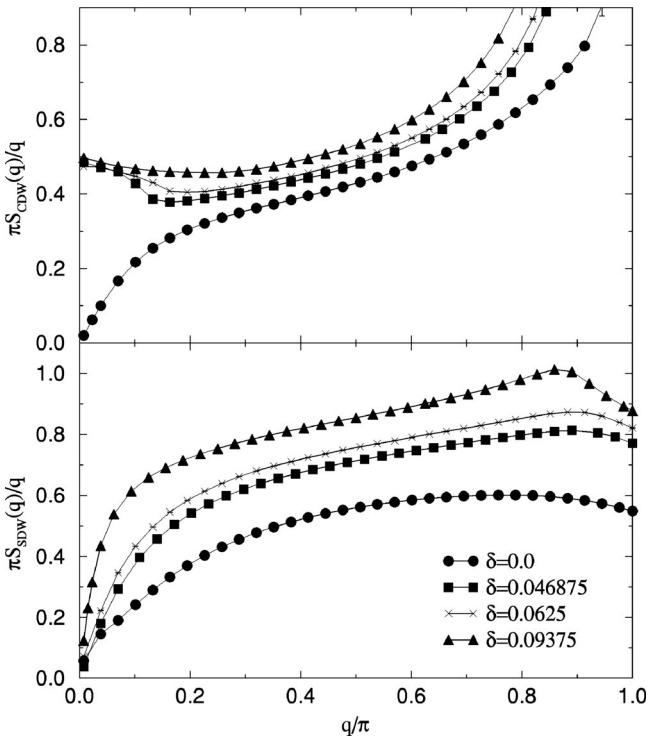

FIG. 16. Same as Fig. 15 for $U=4$, $V=2.5$, where the half-filled system is in the CDW phase.

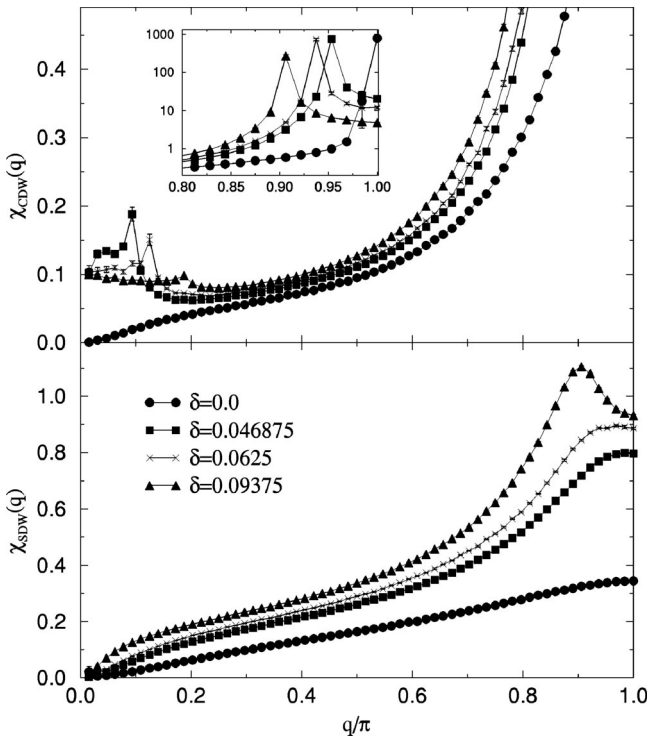

FIG. 17. Static CDW and SDW susceptibilities at different doping levels for $U=4$, $V=2.5$ for a $N=256$ chain. The inset shows the $\chi_{CDW}(2k_F)$ peaks on a more detailed scale.

dence for $\delta=0.0625$ on a log-log scale. For system sizes $N \geqslant 64$, the data is seen to fall on a line with slope ≈ 1.5, consistent with the value $K_\rho \approx 0.5$ extracted above.

As a further test of the Luther-Emery liquid nature of the ground state away from half-filling, we have studied the real-space charge and bond correlations as a function of distance. Figure 19 shows the charge correlation for two different system sizes at a dopant concentration of 6.25% and interaction parameters $U=4$ and $V=2.5$. The ground state at half-filling

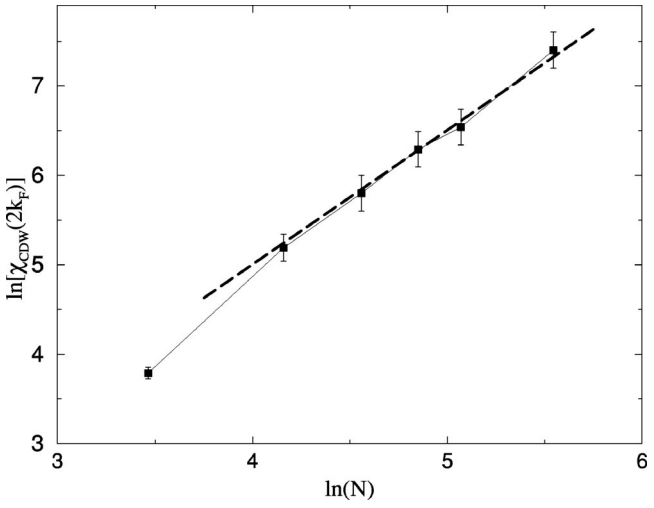

FIG. 18. Finite-size scaling of the static charge susceptibility at $q=2k_F$ for a system with $U=4$, $V=2.5$ at a doping level of 6.25%. A slope of 1.5 is shown by the dashed line.

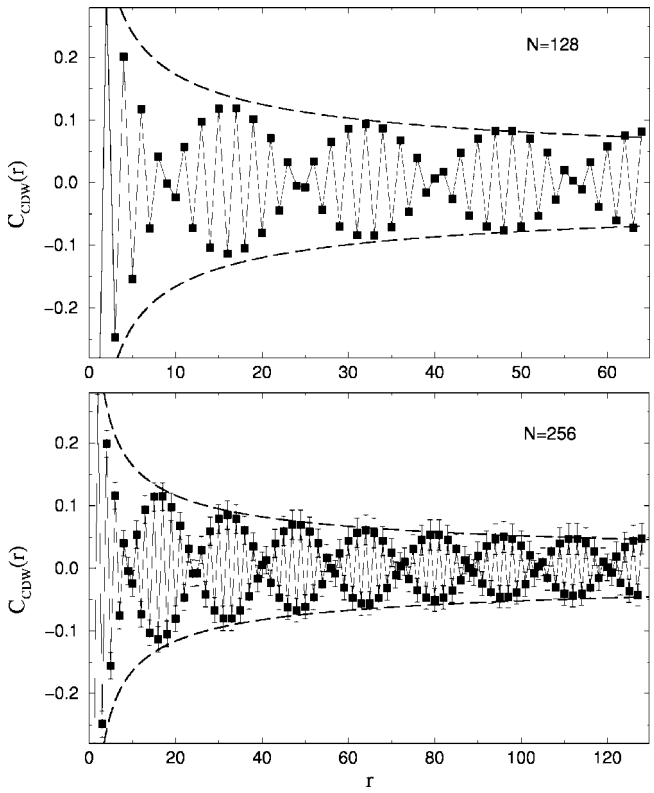

FIG. 19. Real-space charge correlations vs distance at a doping level $\delta=0.0625$ for system sizes $N=128$ and 256 at $U=4$,$V=2.5$.

is a CDW, and for the doped system we find solitonic features with alternating A and B phases separated by domain walls or kinks. However, the correlation decays with distance, and there is no real soliton lattice. In fact, the decay of the magnitude of the peaks is well approximated by an envelope curve of the form $y \sim x^{-0.5}$, and hence also these data are consistent with a Luther-Emery state with $K_\rho \approx 0.5$.

Figure 20 shows a similar plot of the real-space bond-order correlation for $U=4$ and $V=2.14$ at the same dopant concentration and for the same system sizes. The ground state of the half-filled system for this choice of parameters is here a BOW, and away from half-filling, the dominant correlation are still of bond-order type. Once again, the ground state of the doped system has solitonic features with an algebraic decay of the magnitude of the peaks. As in the previous case, the decay is consistent with a Luther-Emery liquid with $K_\rho \approx 0.5$.

V. SUMMARY

To summarize, we have studied the 1D EHM using the SSE method incorporating an efficient operator-loop update and a ''quantum-parallel-tempering'' scheme. Our results confirm the surprising prediction[16] of the existence of a novel long-range-ordered BOW phase between the well-known CDW and SDW phases in the ground-state phase diagram for small to intermediate values of the on-site interaction U ($U<U_m$). We have presented several ways to detect the spin and charge gaps expected in the BOW phase and have also probed directly the BOW correlations and concluded that true long-range order develops. We have studied

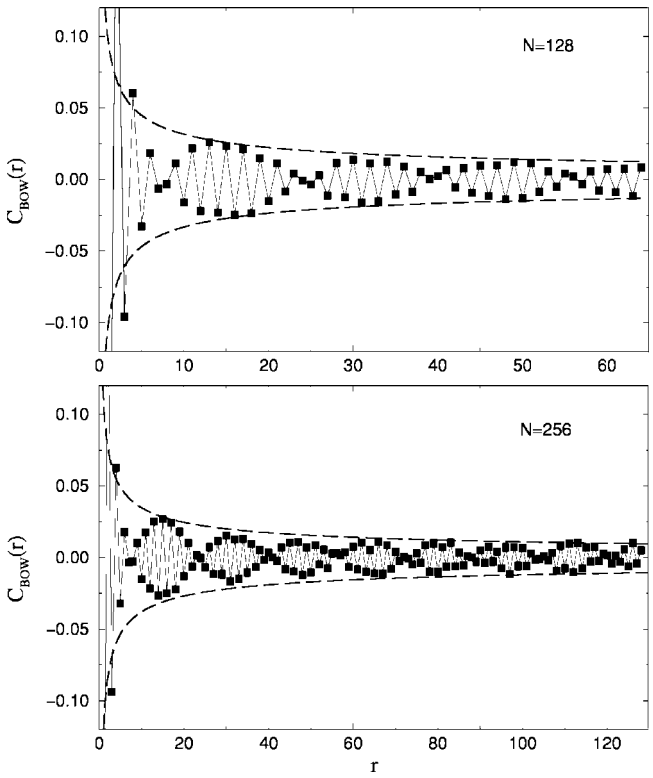

FIG. 20. Bond-order correlations at $\delta=0.0625$, $U=4$,$V=2.14$, for system sizes $N=128$ and 256.

a few points on the BOW-CDW phase boundary and obtained a very good agreement with Nakamura's level-crossing prediction[16] for the location of this phase boundary. For the SDW-BOW phase boundary, our results indicate a higher critical V for fixed U than given by the level crossing method and thus overall a slightly smaller size of the BOW phase. Our results are for significantly larger systems than in the previous study and it is not surprising that the finite-size effects in the level crossings can be large for the SDW-BOW transition since the spin gap opens exponentially slowly in this Kosterlitz-Thouless transition. An overestimation of the size of the BOW phase from the level crossings is also apparent considering that our estimated multicritical point is well within the BOW phase of Nakamura's phase diagram. Since our BOW-CDW phase boundaries agree, this indicates problems with the scaling of the exact SDW-BOW level crossings close to the multicritical point, as was also mentioned by Nakamura.[16] For large values of U ($U>U_m$) the transition is discontinuous (first order). We have shown that curves of the CDW order parameter across this boundary for different system sizes cross each other twice, and explained this behavior in terms of an avoided level crossing. We have also used the curve crossings as a means to locate the position of the multicritical point with greater accuracy than previously attained. Our estimate for the multicritical point is $U_m=4.7\pm0.1$, $V_m=2.51\pm0.04$.

We have also studied systems doped slightly away from half-filling. We find that both the doped CDW and BOW states give rise to ground states of the Luther-Emery type, i.e., the quantum fluctuations do not allow the formation of true soliton lattices. Based on the fact that the BOW state is very similar to the dimerized ground state of models with finite-frequency (nonadiabatic) phonons, we conjecture that the soliton lattice is also unstable to arbitrarily weak quantum fluctuations in these models, unless two- or three-dimensional couplings are taken into account.

After our completion of the numerical calculations at half-filling Tsuchiizu and Furusaki[44] presented a weak-coupling g-ology calculation taking into account second-order corrections to the coupling constants. They obtained a phase diagram in very good quantitative agreement with ours, including the location of the multicritical point.

ACKNOWLEDGMENTS

We would like to thank R. T. Clay for discussions of the operator-loop update for fermions. We thank M. Nakamura for sending us some of his numerical results for comparisons. A.W.S. would like to thank O. Sushkov for discussions. This work was supported by the NSF under Grant No. DMR-97-12765 and by the Academy of Finland (project 26175). Most of the numerical calculations were carried out on the SGI Origin2000 and Condor systems at the NCSA, Urbana, Illinois. Some simulations were also carried out on the Origin2000 at CSC - Scientific Computing Ltd. in Helsinki.

APPENDIX A: OPERATOR-LOOP UPDATES IN THE SSE METHOD

The basic SSE approach has been discussed in several papers.[17–19] We here start with a brief review as a basis for introducing the operator-loop update[19] in the context of fermion models.

To implement the SSE method, the Hamiltonian (1) is written, up to an additive constant, in the form

$$H=-\sum_{b=1}^{N}(H_{1,b}+H_{2,b}+H_{3,b}), \tag{A1}$$

where b is the bond connecting the sites b and $b+1$, N is the length of the chain, and the operators $H_{a,b}$, $a=1,2,3$ are defined as

$$\begin{aligned} H_{1,b}&=C-\frac{U}{2}\left(n_{b,\uparrow}-\frac{1}{2}\right)\left(n_{b,\downarrow}-\frac{1}{2}\right)-\frac{U}{2}\left(n_{b+1,\uparrow}-\frac{1}{2}\right)\\ &\times\left(n_{b+1,\downarrow}-\frac{1}{2}\right)-V(n_b-1)(n_{b+1}-1),\\ H_{2,b}&=t(c^{\dagger}_{b+1,\downarrow}c_{b,\downarrow}+\text{H.c.}),\\ H_{3,b}&=t(c^{\dagger}_{b+1,\uparrow}c_{b,\uparrow}+\text{H.c.}). \end{aligned} \tag{A2}$$

The constant C shifts the zero of the energy and is chosen to ensure a non-negative expectation value for $H_{1,b}$ (needed in order to ensure a positive definite expansion of the partition function). Introducing a basis $\{|\alpha\rangle\}=\{|\zeta_1,\zeta_2,\ldots,\zeta_N\rangle\}$, where $\zeta_i\in\{0,\uparrow,\downarrow,\uparrow\downarrow\}$ denotes the electron state at the site i, the partition function $Z=\mathrm{Tr}\{e^{-\beta H}\}$ can be expanded in a Taylor series as

$$Z=\sum_{\alpha}\sum_{n=0}^{\infty}\sum_{S_n}\frac{\beta^n}{n!}\langle\alpha|\prod_{p=1}^{n}H_{a_p,b_p}|\alpha\rangle, \tag{A3}$$

where S_n denotes a sequence of index pairs defining the operator string $\Pi_{p=1}^{n}H_{a_p,b_p}$

$$S_n=[a,b]_1[a,b]_2\cdots[a,b]_n, \tag{A4}$$

where we use the notation $[a,b]_p=[a_p,b_p]$ and $a\in\{1,2,3\}$, $b\in\{1,\ldots,N\}$. In order to construct an efficient updating scheme, the Taylor series is truncated at a self-consistently determined power L, large enough to cause only an exponentially small, completely negligible error ($L\sim\beta|E|$, where E is the total internal energy; for details see Refs. 17 and 18). We can then define a sampling space where the length of the sequences is fixed, by inserting $L-n$ unit operators, denoted by $H_{0,0}$, into each sequence. The terms in the partition function must be divided by $\binom{L}{n}$ in order to compensate for the different ways of inserting the unit operators. The summation over n is then implicitly included in the summation over all sequences of length L. The partition function takes the form

$$Z=\sum_{\alpha}\sum_{S_L}\frac{\beta^n(L-n)!}{L!}\left\langle\alpha\left|\prod_{p=1}^{L}H_{a_p,b_p}\right|\alpha\right\rangle, \tag{A5}$$

where the operator-index pairs $[a,b]_p$ now have $a\in\{1,2,3\}$ and $b\in\{1,\ldots,N\}$ or $[a,b]_p=[0,0]$. For convenience, we introduce a notation for states obtained by the action of the first p elements of the operator string S_L

$$|\alpha(p)\rangle\sim\prod_{j=1}^{p}H_{a_j,b_j}|\alpha\rangle. \tag{A6}$$

For a nonzero contribution to the partition function, $|\alpha(L)\rangle=|\alpha(0)\rangle$.

A Monte Carlo scheme is used to sample the configurations (α,S_L) according to their relative contributions (weights) to Z. The sampling scheme consists of two types of updates,[17–19] referred to as diagonal update and operator-loop updates. The diagonal update involves local substitutions of the form $[0,0]_p\leftrightarrow[1,b]_p$ and is attempted consecutively for every $p\in\{1,\ldots,L\}$ in the sequence for which $[a,b]_p=[0,0]_p$ or $[1,b]_p$. The updates are accepted with probabilities

$$P([0,0]_p\rightarrow[1,b]_p)=\frac{N\beta M_{1,b}(p)}{L-n},$$

$$P([1,b]_p\rightarrow[0,0]_p)=\frac{L-n+1}{N\beta M_{1,b}(p)}, \tag{A7}$$

where

$$M_{a,b}(p)=\langle\zeta_b(p),\zeta_{b+1}(p)|H_{a,b}|\zeta_b(p-1),\zeta_{b+1}(p-1)\rangle \tag{A8}$$

is a matrix element on bond b, which in this case is diagonal ($a=1$). Only a single state $|\alpha(p)\rangle$ is stored in the computer during the diagonal update. When off-diagonal operators are encountered during the successive scanning of the operator string, the corresponding electron states are updated so that the information needed for evaluation of the probabilities (A7) is always available when needed.

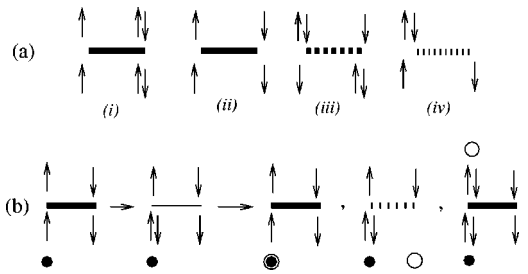

FIG. 21. (a) A few allowed vertices. The solid lines denote the diagonal Hamiltonian operator, the dashed and dotted lines denote the hopping operators for the up and down spins, respectively. The lower legs denote the states $\zeta_i(p-1)$ and $\zeta_{i+1}(p-1)$ while the upper legs denote $\zeta_i(p)$ and $\zeta_{i+1}(p)$. (b) An example of a vertex update. The entrance leg is the lower left leg of the vertex, as indicated by the dot. The electron state at the entrance leg $\uparrow$ is changed to $\uparrow\downarrow$ in this particular update. Given that, the three possible resulting vertices are shown. The corresponding exit legs are denoted by open circles. Exit at the upper right leg does not result in an allowed vertex in this case.

The operator-loop update has been discussed in detail in Ref. 19 in the context of spins. Here we present the construction of loops for fermions. As explained in Ref. 19, the matrix element in Eq. (A5) can be graphically represented by a set of n vertices (corresponding to the n nonunit operators in S_L) connected to one another by the propagated electron states [see Fig. 21(a)]. Each vertex has four ''legs'' with electron states $|\zeta_i(p-1),\zeta_{i+1}(p-1)\rangle$ and $|\zeta_i(p),\zeta_{i+1}(p)\rangle$ before and after the action of the associated Hamiltonian operator H_{a_p,b_p}. There are 32 allowed vertices—16 diagonal ones and eight each associated with the off-diagonal $H_{2,b}$ and $H_{3,b}$. A configuration (α,S_L) is completely specified by the leg states of the n vertices—except for sites that do not have any operators acting on them.

To carry out the operator-loop update, the linked list of the n vertices is first constructed. In addition to the electron states at the legs of each vertex, the list also contains the addresses (i.e., the location in S_L) of the next vertex and the corresponding leg that each leg is connected to. The loop construction begins with randomly choosing a vertex and an ''entry'' leg. The electron state at the entry leg is changed to one of the three other allowed states chosen at random. Next an ''exit'' leg is chosen (following a procedure described below) and its associated electron state is updated so that the new leg states constitute an allowed vertex [see Fig. 21(b)]. The exit leg will be linked to a leg of another vertex (or, if there is only one operator in the configuration that acts on the site in question, another leg on the same vertex) and this will be the entry leg for the next vertex. The electron state at this new entry leg is then updated to match the state at the exit leg of the previous vertex. A new exit leg is then chosen following the same procedure. This is repeated until the exit leg from a vertex points to the starting point of the loop,

which implies that the loop is closed and a new allowed configuration has been generated.

To choose an exit leg—given a vertex, an entry leg and the updated electron state at the entry leg—all the legs can be considered in turn and attempts made to update the associated electron state so that the new leg states constitute an allowed vertex. Because of spin and charge conservation on the vertices, at a given exit leg there is at most one possible update of the electron state that can lead to an allowed vertex. Hence, the exit leg uniquely determines the new vertex and the probability of choosing a given leg should be proportional to the weight of the new vertex, i.e., a matrix element of the form (A8), which in this case can be either diagonal or off-diagonal. In practice, a fast selection of an exit leg and updating of the vertex state is achieved using two pregenerated tables. The first one contains the cumulative probabilities of the four exit legs given an entrance leg, the old vertex state, and the new state at the entrance. The second table contains the new vertex states corresponding to the updated entrance and exit legs.

A special case occurs if the initial update at the entry leg of the first vertex of a loop is a spin flip, i.e., the electron state changes from $\uparrow$ to $\downarrow$ or vice versa. In this case, the vertex weight does not change when updated and as a consequence the ''bounce process,'' where the exit leg is the same as the entrance leg, does not have to be included in the loop construction. The loop then becomes deterministic, i.e., there is a unique exit leg given by the entrance leg.[19] This is similar to the ''loop-exchange'' algorithm proposed in the context of the world-line method.[45]

A full Monte Carlo updating cycle (MC step) consists of a diagonal update, followed by the construction of a linked vertex list. Next a number of operator-loop updates are carried out and finally the vertices are mapped back into a corresponding sequence S_L. The loop update typically also implies changes in the stored state $|\alpha\rangle=|\alpha(0)\rangle$, as some of the vertex legs (links) span across the periodic boundary in the propagation direction. The number of up and down electrons can be changed by the operator-loop update, as can the spatial winding numbers, and the algorithm is hence fully grand canonical. Note that at high and moderately low temperatures there are typically some sites of the system, which has no vertices associated with them. The states on these sites can be randomly changed, since they have no effect on the configuration weight.

The number of loops constructed for every MC step is determined such that on an average a total of $\sim L$ vertices (we typically use $2L$) are visited. The truncation L and the number of loops are adjusted during the equilibration part of the simulation and are thereafter held fixed. L is determined by requiring that the highest n reached during equilibration is at most 70–80 % of L.

In certain parameter regions, the length of a loop can sometimes become extremely long before it closes—in practice, it may even never close. It is, therefore, necessary to impose a maximum length, beyond which the loop construction is terminated and a new starting point is chosen (typically, we use $\sim 50L$ for this cut-off length). In order to reduce the likelihood of the next loop also exceeding the termination length, it has proven useful to carry out a diagonal update before starting the next loop. The loop termination does not violate detailed balance and does not cause any systematical errors in the results. In most cases, incomplete loop termination occurs so infrequently that it does not adversely affect the simulation. In analogy with Ref. 46, where a scheme (there called ''worm'' update) similar to the operator loops considered here was first introduced within the continuous world-line representation, the end points of the loop during construction can be related to the single-particle Green's function of the system and hence the tendency for loops to become exceedingly long for some parameter values must be related to some physical properties of the system. This issue should be studied further.

Estimators for the various structure factors and susceptibilities have been discussed in previous papers.[17,18] Here we only note that the charge and spin stiffness constants, Eq. (6), can be expressed in terms of spin and charge current operators in analogy with the spin stiffness of the Heisenberg antiferromagnet previously discussed in Ref. 18, leading to

$$\rho_{c,s}=\frac{[(n_R^{\uparrow}-n_L^{\uparrow})\pm(n_R^{\downarrow}-n_L^{\downarrow})]^2}{N\beta}, \tag{A9}$$

where $n_{R,L}^{\sigma}$ is the number of kinetic-energy operators in the SSE term propagating spin-σ particles in the ''right'' and ''left'' direction on the ring. Because of spin and charge conservation, the topological winding numbers $(n_R^{\sigma}-n_L^{\sigma})/N$ can take only integer values.

Although the operator-loop algorithm very significantly speeds up SSE simulations, in many cases reducing the autocorrelation function by orders of magnitude, the dynamics is still very slow in some parameter regions. For the extended Hubbard model studied here, problems with very long autocorrelation times occur in the long-range-ordered BOW and CDW phases. The problems are particularly severe for large systems close to the BOW-CDW phase boundary, where ''trapping''in the wrong phase often occurs. The slow dynamics in the BOW phase is illustrated in Fig. 22, which shows the simulation time dependence of $S_{BOW}(\pi)$ and $\chi_{BOW}(\pi)$ during a simulation of a 256-site system at $\beta=512$ [S_{BOW} has converged at this β but χ_{BOW} is about 20% larger still at $\beta=1024$]. It is evident that the BOW autocorrelation time here is tens of thousands of MC steps. The BOW susceptibility exhibits a behavior where it sometimes takes very small values (less than 10^{-3} of the average value), but corresponding large fluctuations upwards do not occur, i.e., the distribution of the $\chi_{BOW}(\pi)$ estimator for individual configurations is very skewed. The structure factor exhibits a more symmetric distribution. This behavior can be understood as a consequence of the BOW ground state for a finite system being a symmetric combination of the two possible real-space symmetry-broken states. The symmetry is not broken in a finite system and the simulation is also not trapped in one of the real-space states. Hence, the wave function that is sampled in the simulation contains both the real-space states and the behavior seen in Fig. 22 indicates that individual configurations also contain both components, in such a way that transitions (''tunneling'') between the two real-

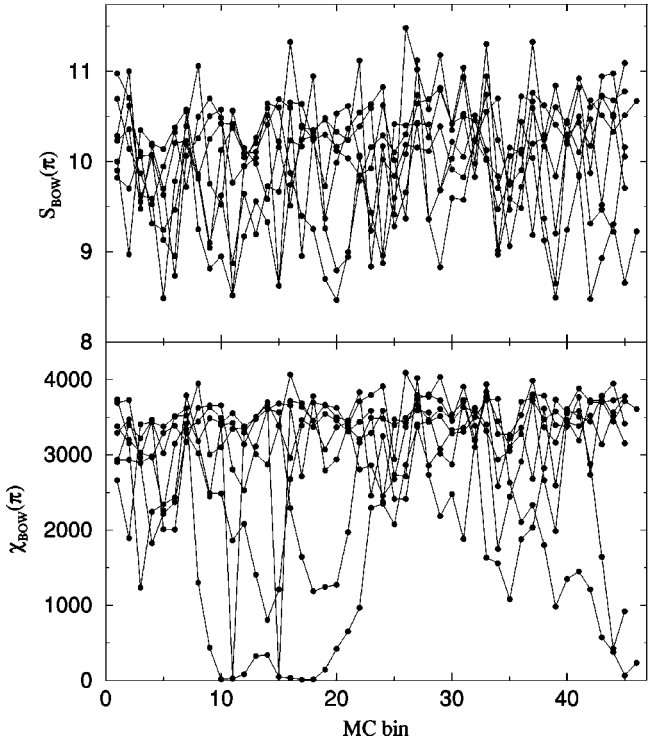

FIG. 22. BOW structure factor and susceptibility for a 256-site system with $U=4$ and $V=2.14$ at inverse temperature $\beta=512$. Results of six independent simulations are shown. Each point represents an average over a bin consisting of 10^4 Monte Carlo steps.

space states can occur during the SSE propagation (which can be simply related[47] to a propagation in imaginary time), at least for some configurations. Tunneling can be inferred from the qualitatively different evolutions of the structure factor and the susceptibility in MC time. The susceptibility is an integral of the bond-order correlation, as in Eq. (4), which in configurations where tunneling occurs can be much smaller than in configurations with no tunneling, since correlations between states with the same real-space configuration contributes positively but correlations between different states give a negative contribution. The structure factor, on the other hand, is an equal time correlation function and would not be reduced much by tunneling if the tunneling times are short. This explains the qualitatively different distributions of the χ_{BOW} and S_{BOW} measurements in Fig. 22. Evidently, the updating process is very slow in adding and removing tunneling events in the configurations, which, maybe, is not that surprising considering that the tunneling is between two states with a discrete broken symmetry. These problems do not occur in SSE simulations of systems with a broken continuous symmetry, such as the two-dimensional Heisenberg model.

The trapping and tunneling problems can be significantly reduced by using the parallel tempering scheme (or exchange Monte Carlo),[20–22] which is discussed below in Appendix B.

APPENDIX B: QUANTUM PARALLEL TEMPERING

The ''quantum-parallel-tempering'' scheme is a straightforward generalization of the thermal-parallel-tempering[20–22] method commonly used to equilibrate classical spin glass simulations. Our implementation amounts to running several simulations simultaneously on a parallel computer, using a fixed value of U and different but closely spaced values of V. Along with the usual Monte Carlo updates, we attempt to swap the configurations for processes with adjacent values of V at regular intervals, typically after every Monte Carlo step, according to a scheme that maintains detailed balance in the extended ensemble of parallel simulations. The probability of swapping the V values of runs i and $i+1$, which are running at V_i and V_{i+1}, respectively, before the swap, is

$$P_{\text{swap}}(V_i, V_{i+1}) = \min\left[1, \frac{W_i(V_{i+1})W_{i+1}(V_i)}{W_i(V_i)W_{i+1}(V_{i+1})}\right], \quad \text{(B1)}$$

where $W_i(V)$ is the SSE weight of the ith simulation configuration evaluated with the coupling V. The swap probabilities for fixed $\Delta V = V_{i+1} - V_i$ decreases with increasing system size and decreasing temperature and hence ΔV and the range of V values (if the number of processes is fixed) must be chosen smaller for larger system sizes.

The computational effort required for the swapping process is very minor compared to the actual quantum Monte Carlo simulations. It is, therefore, useful to carry out several swap attempts of all pairs of neighboring simulations between every MC step. Histograms containing the number of times each of the current configurations has ''occupied'' each V bin can then be constructed and used for adding the con-

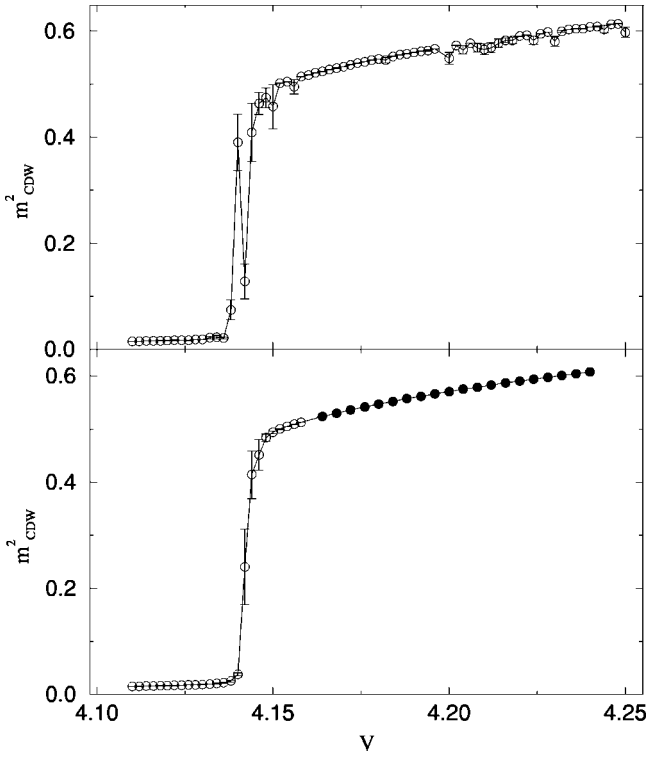

FIG. 23. CDW order parameter across the SDW-CDW phase boundary for $U=8$ ($N=64$, $\beta=64$). The upper panel shows data from individual runs. The lower panel shows the same data obtained using quantum parallel tempering, with two independent runs as indicated by the open and solid circles.

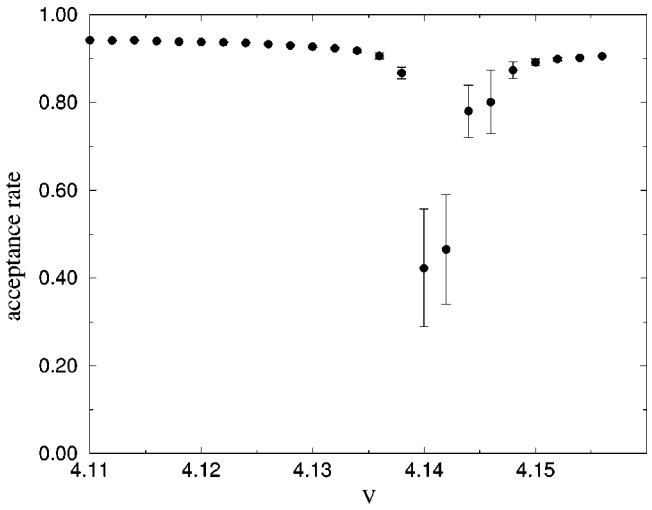

FIG. 24. Tempering acceptance rate during the simulation across the first-order SDW-CDW phase boundary.

tributions of each configuration to all the V bins. This can contribute to reducing the statistical error of measured quantities.

To illustrate the advantage of quantum parallel tempering, we show two sets of data—obtained with and without the use of tempering—for a system undergoing a first-order transition. Figure 23 shows the CDW order parameter across the first-order SDW-CDW phase boundary at $U=8$. The upper panel shows the data obtained from individual runs; the lower panel shows data for the same parameters obtained using tempering. The length of the individual simulations was 10^5 MC steps for all V values, and this was also the number of steps performed by each process in the tempering runs. The improvement in the quality of the tempering data is evident, especially close to the transition point where two of the individual simulations have relaxed into the wrong phases. The statistical errors are hence severely underestimated due to the failure to equilibrate properly within the simulation time. The tempering error bars are also large at the phase transition, but in contrast to those of the individual simulations they are accurate error estimates. The errors rapidly become much smaller as one moves away from the transition point. The effects of tempering are also favorable further inside the CDW phase, where several of the individual simulations are apparently affected by trapping in configurations with defects, where the order is reduced.

The tempering acceptance rate during the run spanning across the phase transition in Fig. 23 is shown in Fig. 24. There is a sharp reduction in the acceptance rate at the transition. This reflects the rapid change in the SSE configurations across the phase boundary, which implies that the configuration weights evaluated with V values from the ''wrong'' phase are likely to decrease and the swap according to the probability (B1) will be rejected.

Finally, we note that tempering, in general, is an application where a superlinear speed-up can be achieved in practice on parallel computers. In addition to doubling the density of data points when the number of processes is doubled, the statistical errors are also reduced. Sometimes the error reduction can be dramatic, but even in cases where there are no real problems with the dynamics of individual simulations the effects of tempering are often very favorable.

[1] V.J. Emery, S.A. Kivelson, and O. Zachar, Phys. Rev. B **56**, 6120 (1997).
[2] *Conjugated Conducting Polymers*, edited by H. G. Keiss (Springer-Verlag, Berlin, 1992).
[3] T. Ishiguro and K. Yamaji, *Organic Superconductors* (Springer-Verlag, Berlin, 1990).
[4] E.H. Lieb and F.Y. Wu, Phys. Rev. Lett. **20**, 1445 (1968).
[5] R.A. Bari, Phys. Rev. B **3**, 2662 (1971).
[6] V.J. Emery, in *Highly Conducting One-Dimensional Solids*, edited by J. T. Devreese, R. Evrand, and V. van Doren (Plenum, New York, 1979), p. 327.
[7] J. Sólyom, Adv. Phys. **28**, 201 (1979).
[8] J.E. Hirsch, Phys. Rev. Lett. **53**, 2327 (1984).
[9] J.E. Hirsch, Phys. Rev. B **31**, 6022 (1985).
[10] J.W. Cannon and E. Fradkin, Phys. Rev. B **41**, 9435 (1990).
[11] J.W. Cannon, R.T. Scalettar, and E. Fradkin, Phys. Rev. B **44**, 5995 (1991).
[12] P.G.J. van Dongen, Phys. Rev. B **49**, 7904 (1994).
[13] B. Fourcade and G. Spronken, Phys. Rev. B **29**, 5096 (1984).
[14] J. Voit, Phys. Rev. B **45**, 4027 (1992).
[15] H.Q. Lin, E.R. Gagliano, D.K. Campbell, E.H. Fradkin, and J.K. Gubernatis, in *Proceedings of the 1993 NATO ARW on the Physics and Mathematical Physics of the Hubbard Model*, edited by D. Baeriswyl *et al.* (Plenum, New York, 1995).
[16] M. Nakamura, J. Phys. Soc. Jpn. **68**, 3123 (1999); Phys. Rev. B **61**, 16 377 (2000).
[17] A.W. Sandvik and J. Kurkijärvi, Phys. Rev. B **43**, 5950 (1991); A.W. Sandvik, J. Phys. A **25**, 3667 (1992).
[18] A.W. Sandvik, Phys. Rev. B **56**, 11 678 (1997).
[19] A.W. Sandvik, Phys. Rev. B **59**, R14 157 (1999).
[20] K. Hukushima, H. Takayama, and K. Nemoto, Int. J. Mod. Phys. C **7**, 337 (1996).
[21] K. Hukushima, K. Nemoto, J. Phys. Soc. Jpn. **65**, 1604 (1996).
[22] E. Marinari, in *Advances in Computer Simulation*, edited by J. Kertsz and I. Kondor, Lecture Notes in Physics Vol. 501 (Springer, Berlin, 1998).
[23] P.V. Shevchenko, A.W. Sandvik, and O.P. Sushkov, Phys. Rev. B **61**, 3475 (2000).
[24] S. Wessel, B. Normand, M. Sigrist, and S. Haas, Phys. Rev. Lett. **86**, 1086 (2001).
[25] A. Dorneich and M. Troyer, Phys. Rev. E **64**, 066701 (2001).
[26] W. Kohn, Phys. Rev. A **133**, A171 (1964).
[27] Strictly speaking, our boundary conditions are antiperiodic, which is what one automatically obtains at half-filling when the system size N is a multiple of 4 and the fermion anticommutation relations giving negative signs from transport across the boundary are neglected.

[28] J. Voit, Rep. Prog. Phys. **57**, 977 (1994).
[29] R.T. Clay, A.W. Sandvik, and D.K. Campbell, Phys. Rev. B **59**, 4665 (1999).
[30] H.J. Schulz, Phys. Rev. Lett. **64**, 2831 (1990); Int. J. Mod. Phys. **5**, 57 (1991).
[31] F. Woynarovich and H.-P. Eckle, J. Phys. A **20**, L97 (1987).
[32] S. Eggert, I. Affleck, and M. Takahashi, Phys. Rev. Lett. **73**, 332 (1994).
[33] S. Eggert, Phys. Rev. B **54**, R9612 (1996).
[34] H. Weber and P. Minnhagen, Phys. Rev. B **37**, 5986 (1987); K. Harada and N. Kawashima, J. Phys. Soc. Jpn. **67**, 2768 (1998).
[35] A.W. Sandvik and D.K. Campbell, Phys. Rev. Lett. **83**, 195 (1999).
[36] K. Nomura and K. Okamoto, J. Phys. A **27**, 5773 (1994); J.L. Cardy, *ibid.* **20**, L891 (1987).
[37] A. Luther and V.J. Emery, Phys. Rev. Lett. **33**, 589 (1974).
[38] A.W. Sandvik and D.J. Scalapino Phys. Rev. B **47**, 12 333 (1993); A.W. Sandvik, D.J. Scalapino, and C. Singh, *ibid.* **48**, 2112 (1993).
[39] W.P. Su, J.R. Schrieffer, and A.J. Heeger, Phys. Rev. Lett. **42**, 1698 (1979); Phys. Rev. B **22**, 2099 (1980).
[40] M.I. Salkola and S.A. Kivelson, Phys. Rev. B **50**, 13 962 (1994).
[41] E. Jeckelmann, Phys. Rev. B **57**, 11 838 (1998).
[42] E. Fradkin and J.E. Hirsch, Phys. Rev. B **27**, 1680 (1983); J.E. Hirsch and E. Fradkin, Phys. Rev. B **27**, 4302 (1983).
[43] Since we work on a periodic lattice, $4k_F = 2\pi\delta$ and $2k_F = \pi(1 - \delta)$.
[44] M. Tsuchiizu and A. Furusaki, cond-mat/0109051 (unpublished).
[45] N. Kawashima, J.E. Gubernatis, and H.G. Evertz, Phys. Rev. B **50**, 136 (1994).
[46] N.V. Prokof'ev, B.V. Svistunov, and I.S. Tupitsyn, Zh. Eksp. Teor. Fiz. **64**, 853 (1996); JETP **87**, 310 (1998).
[47] A.W. Sandvik, R.R.P. Singh, and D.K. Campbell, Phys. Rev. B **56**, 14510 (1997).